Monthly Notices
of the
ROYAL ASTRONOMICAL SOCIETY

MNRAS **451,** 2399–2416 (2015) doi:10.1093/mnras/stv1109

The origin of long-lived asteroids in the 2:1 mean-motion resonance with Jupiter

O. Chrenko,[1⋆] M. Brož,[1⋆] D. Nesvorný,[2] K. Tsiganis[3] and D. K. Skoulidou[3]

[1]*Institute of Astronomy, Charles University in Prague, V Holešovičkách 2, CZ-18000 Prague 8, Czech Republic*
[2]*Department of Space Studies, Southwest Research Institute, 1050 Walnut Street, Suite 300, Boulder, CO 80302, USA*
[3]*Department of Physics, Aristotle University of Thessaloniki, GR-54124 Thessaloniki, Greece*

Accepted 2015 May 12. Received 2015 May 12; in original form 2015 April 4

ABSTRACT

The 2:1 mean-motion resonance with Jupiter harbours two distinct groups of asteroids. The short-lived population is known to be a transient group sustained in steady state by the Yarkovsky semimajor axis drift. The long-lived asteroids, however, can exhibit dynamical lifetimes comparable to 4 Gyr. They reside near two isolated islands of the phase space denoted A and B, with an uneven population ratio $B/A \simeq 10$. The orbits of A-island asteroids are predominantly highly inclined, compared to island B. The size–frequency distribution is steep but the orbital distribution lacks any evidence of a collisional cluster. These observational constraints are somewhat puzzling and therefore the origin of the long-lived asteroids has not been explained so far. With the aim to provide a viable explanation, we first update the resonant population and revisit its physical properties. Using an *N*-body model with seven planets and the Yarkovsky effect included, we demonstrate that the dynamical depletion of island A is faster, in comparison with island B. Then we investigate (i) the survivability of primordial resonant asteroids and (ii) capture of the population during planetary migration, following a recently described scenario with an escaping fifth giant planet and a jumping-Jupiter instability. We also model the collisional evolution of the resonant population over past 4 Gyr. Our conclusion is that the long-lived group was created by resonant capture from a narrow part of hypothetical outer main-belt family during planetary migration. Primordial asteroids surviving the migration were probably not numerous enough to substantially contribute to the observed population.

Key words: methods: numerical – minor planets, asteroids: general.

1 INTRODUCTION

The 2:1 mean-motion resonance with Jupiter, hereinafter denoted as J2/1, is one of the major first-order Jovian resonances intersecting the main asteroid belt. It is associated with the Kirkwood gap known as the Hecuba gap (Kirkwood 1867; Schweizer 1969), which is commonly considered to be the borderline separating the outer main belt and the Cybele region. Its name is derived from (108) Hecuba which is an outer main-belt asteroid but technically does not exhibit the exact 2:1 commensurability (Schubart 1964).

The 2:1 resonance, which was originally believed to be depleted of asteroids, harbours several small-sized bodies as it was realized by observations in the 20th century (the first resonant asteroid (1362) Griqua was recognized in 1943 (Rabe 1959)). The follow-up studies based on analytical and semi-analytical methods (e.g. Murray 1986; Moons, Morbidelli & Migliorini 1998), symplectic mapping (e.g. Roig & Ferraz-Mello 1999) and frequency analysis (e.g. Nesvorný & Ferraz-Mello 1997) helped to get insight to the internal structure of the resonance and to investigate the character of various resonant orbits affected by a complicated interplay between the J2/1 and overlapping secular (Morbidelli & Moons 1993) and secondary resonances (Wisdom 1987; Henrard, Watanabe & Moons 1995). In particular, it was discovered that while the regions of the overlap give rise to a strongly chaotic behaviour of the asteroidal orbits, there are two separate regions of quasi-regular motion located inside the resonant part of the phase space (Franklin 1994; Michtchenko & Ferraz-Mello 1997). These regions were designated as stable islands A and B (Nesvorný & Ferraz-Mello 1997, see e.g. Fig. 1).

However, it was also suggested by Ferraz-Mello, Michtchenko & Roig (1998) that the stability of the islands could have been weakened in the past. The mechanism responsible for this increase of chaos was introduced as 1:1 resonance of the J2/1 libration period with the period of Jupiter–Saturn great inequality (GI). Although the present value of the GI period is 880 yr, it was probably smaller when configuration of planetary orbits was more compact (Morbidelli & Crida 2007) and it slowly increased during Jupiter's and Saturn's divergent migration. If the value of the GI period was temporarily comparable with the libration period of the J2/1 asteroids (which

⋆ E-mail: chrenko@sirrah.troja.mff.cuni.cz (OC);
mira@sirrah.troja.mff.cuni.cz (MB)

is typically $\simeq 420$ yr), the aforementioned resonance would have occurred.

With ongoing improvements of the observation techniques and sky surveys, there is now a population of asteroids inside the J2/1 which is large enough to be analysed statistically with numerical methods. Long-term integrations in a simplified model with four giant planets were performed by Roig, Nesvorný & Ferraz-Mello (2002) who identified both short-lived and long-lived asteroids within the observed population, which consisted of 53 bodies by then. Investigating resident lifetimes of the resonant asteroids, Roig et al. (2002) demonstrated that part of the population escapes from the resonance on time-scales $\sim$10 Myr, while other asteroids may have dynamical lifetimes comparable to the age of the Solar system. The orbits of these long-lived asteroids were embodied in island B and part of them was also present in its boundaries, being affected by chaotic diffusion. Surprisingly, the stable island A was empty.

In a series of papers focused on the 2:1 mean-motion resonance, Brož et al. (2005) and Brož & Vokrouhlický (2008) identified significantly more bodies as resonant. The latter catalogue contained 92 short-lived and 182 long-lived asteroids. They also realized that nine of the long-lived asteroids were located in island A, while the rest was residing in the island B and its vicinity. They successfully explained the origin of the short-lived asteroids by a numerical steady-state model, in which the resonant population was replenished by an inflow of outer main-belt asteroids driven by the Yarkovsky semimajor axis drift. However, this model fails in the case of the long-lived population which was thought to be created by Yarkovsky-induced injection of the nearby Themis family asteroids that exhibit similar inclinations as the B-island asteroids. Brož et al. (2005) showed that the objects transported from Themis are usually perturbed shortly after entering the resonance and rarely reach the islands.

Roig et al. (2002) argued that the steep size–frequency distribution (SFD) of the long-lived asteroids, which was inconsistent with a steady state (Dohnanyi 1969), could imply recent collisional origin. On the contrary, there was no collisional cluster identified in the orbital distribution by Brož & Vokrouhlický (2008), thus a collisional family would have to be older than 1 Gyr. Moreover, the presence of the highly inclined A-island asteroids would require unrealistic ejection velocities, assuming that the disruption occurred in the more populated island B.

As there is no self-consistent explanation, the main goal of this paper is to provide a reasonable model for the formation and evolution of the long-lived population, taking into account the paucity of bodies in island A, the differences in the inclination and the non-equilibrium size distribution.

The long dynamical lifetimes of the dynamically stable asteroids, together with the failure of the aforementioned hypotheses, strongly indicates that their origin may be traced back to the epoch of planetary migration. Recent advances in migration theories suggest that a primordial compact configuration of planetary orbits and subsequent violent planetary migration might have led to a destabilization of several regions that are otherwise stable under the current planetary configuration. The populations of Trojans and Hildas (Nesvorný, Vokrouhlický & Morbidelli 2013) may serve as examples of such a process: the primordial populations in the 1:1 and 3:2 resonances with Jupiter were totally dispersed and the observed populations were formed by resonant capture of bodies, originating either in the outer main belt or in the trans-Neptunian disc of comets. It seems inevitable that the 2:1 resonance with Jupiter also undergoes significant changes of its location, inner secular structure and asteroid population, during the planetary migration.

The structure of the paper is as follows. We first use the latest observational data from the data bases AstOrb, AstDyS, WISE and SDSS to update the observed population in Section 2. We also briefly review the characterization of resonant orbits and describe a method of dynamical mapping. In Section 3, we study whether the planetary migration may cause depletion or repopulation of the long-lived J2/1 asteroids. The dynamical models we create are based on simulations with prescribed evolution of planets in context of the modern migration scenario with five giant planets and *jumping-Jupiter instability* (Nesvorný & Morbidelli 2012). Section 4 is focused on dynamical simulations covering the late stage of planetary migration during which the GI period evolution might have influenced the stability of the long-lived asteroids. In Section 5, we examine the effects of collisions on the long-lived population. Finally, Section 6 is devoted to conclusions.

2 OBSERVED RESONANT POPULATION

In this section, we first describe methods we use for identification and description of resonant orbits as well as for dynamical mapping of the resonance. Our approach is similar to the one used by Roig et al. (2002). We identify resonant orbits in a recent catalogue of osculating orbital elements and we study their dynamical lifetimes on the basis of long-term numerical integrations in a simplified model with four giant planets only. Our goal is also to survey available data for physical properties of the population, namely the absolute magnitudes, sizes and albedos. In the last subsection, we revisit results of Skoulidou et al. (in preparation) in order to compare the simplified four-giant-planet model with a more sophisticated framework including terrestrial planets and the Yarkovsky effect. Especially, we look for the differences in the dynamical decay rates in the stable islands A and B.

2.1 Characterization of resonant orbits

The 2:1 resonance critical angle is defined as

$$\sigma \equiv 2\lambda_{\rm J} - \lambda - \varpi \,, \tag{1}$$

where $\lambda_{\rm J}$ and λ are the mean longitudes of Jupiter and of an asteroid, respectively, ϖ is the asteroid's longitude of perihelion. The critical argument of any body trapped inside the J2/1 resonance librates (quasi-periodically changes on an interval $< 2\pi$) with a typical period of about 420 yr. On the other hand, the critical argument of the asteroids outside the resonance circulates. This provides us a useful tool for the identification of the resonant asteroids.

The libration of σ is linked to periodic changes of the osculating semimajor axis a, the eccentricity e and the inclination I. These changes are coupled together as described by the adiabatic invariant N of the asteroid's motion in the circular and planar restricted Sun–Jupiter–asteroid system:

$$N = \sqrt{a}\left(2 - \sqrt{1-e^2}\cos I\right) \,. \tag{2}$$

The presence of other planets and variable eccentricity of Jupiter's orbit give rise to multiple perturbations in the J2/1 and prevent integrability of the orbits.

None the less, the a, e, I coupling is preserved to a certain degree. Semimajor axis oscillates around the libration centre, which is positioned approximately at the exact resonance $a_{\rm res} \simeq 3.27$ au.

The eccentricity and inclination attain their maximal values when the oscillation of a is at its minimum and vice versa.

An inconvenient consequence of this behaviour is that the standard averaging methods for the computation of proper elements (Knežević & Milani 2003) do not retain any information about the libration amplitude (i.e. the proper semimajor axes of all resonant asteroids approach the value of $a_{\rm res}$). Therefore the proper elements are not the appropriate choice when studying resonant orbits.

In order to properly characterize the libration amplitude, we use an alternative set of resonant (or pseudo-proper) elements (Roig et al. 2002). The idea is to record the osculating orbital elements at the moment when they reach their extremal values during the libration cycle. These values can be found as the intersections with a suitably defined reference plane in the osculating elements space. A set of conditions determining this plane can be written as

$$\sigma = 0 \wedge \frac{{\rm d}\sigma}{{\rm d}t} > 0 \wedge \varpi - \varpi_{\rm J} = 0 \wedge \Omega - \Omega_{\rm J} = 0\,, \tag{3}$$

where Ω denotes the longitude of node and subscript J is used for Jupiter. The purpose of the conditions for ϖ and Ω is to eliminate secular variations of the resonant elements. The whole set enables the resonant elements to be recorded when the osculating semimajor axis a reaches its minimum, the eccentricity e and the inclination I attain maxima. Note that as a consequence, the J2/1 asteroids are always depicted on the left-hand side (closer to the Sun) of the libration centre in the resonant elements space (see e.g. Fig. 2).

Moreover, temporal evolution of resonant elements may serve as the first indicator of the stability. The reason is that stable orbits exhibit stable libration with only a small variation around the mean value. Therefore, successive intersections with the reference plane do not move significantly and the recorded resonant elements are nearly exact constants of motion. The situation for the unstable orbits is just the opposite and the intersections slowly disperse in time. This fact propagates numerically to the resulting resonant elements, if we compute their standard deviation as an error of the mean value obtained over a significant period of time (∼100 kyr).

Nevertheless, due to higher order perturbations and secular effects, the above conditions are seldom satisfied exactly and one has to use less-confined criteria in the following form when numerically integrating the orbits:

$$|\sigma| < 5^\circ \wedge \frac{\Delta\sigma}{\Delta t} > 0 \wedge |\varpi - \varpi_{\rm J}| < 5^\circ\,. \tag{4}$$

We use the difference between successive numerical time steps (denoted as $\Delta\sigma$) rather than the time derivative. Note that we completely omit the condition for Ω. This simplification can be compensated by verifying that the maximal value of the inclination is reached when recording the resonant elements.

2.2 Dynamical maps

In this section, we summarize our approach to dynamical mapping of the 2:1 resonance and its secular structure. Our method is verified by comparing the map computed for the present configuration of planets with the separatrices and locations of secular resonances derived by Moons et al. (1998). An important outcome is our ability to record global changes inside the resonance when the planetary orbits are reconfigured and also to examine dynamical stability in various regions of the resonant phase space.

Our method employs the definition of the resonant elements. The respective values should change systematically in the case of unstable resonant orbits, whereas stable orbits should only oscillate with small variations. The same behaviour is exhibited by actions of a dynamical system; time series of their extremal or mean values are therefore often used for dynamical mapping (e.g Laskar 1994; Morbidelli 1997; Tsiganis, Knežević & Varvoglis 2007).

We proceed as follows. First, we divide an investigated part of the phase space into the boxes of the same size. Let the central coordinates (a, e, I) of each box represent a set of initial resonant elements (this is accomplished by setting the osculating angular elements so that condition (3) is fulfilled). We integrate the initial orbits over several millions of years and track the evolution of the resonant elements. Finally, we determine the differences $\delta a_{\rm r}$, $\delta e_{\rm r}$ and $\delta \sin I_{\rm r}$ between the initial and final (or the last recorded) resonant elements. These values represent the dynamical stability of the initial orbit and we use them as characteristics of the entire box.

For the purpose of expressing the total displacement in the phase space, we define the distance

$$d \equiv \sqrt{\left(\frac{\delta a_{\rm r}}{\bar{a}_{\rm r}}\right)^2 + (\delta e_{\rm r})^2 + (\delta \sin I_{\rm r})^2}\,, \tag{5}$$

where $\bar{a}_{\rm r}$ denotes the arithmetic mean of the initial and final resonant semimajor axis. The distance d is similar to the metric used in the Hierarchical Clustering Method (Zappalà et al. 1995) for family identification.

In order to verify our method, we constructed a dynamical map of the 2:1 resonance in the *present* configuration of planets. We investigated the phase space in the intervals $a \in (3.195, 3.275)$ au, $e \in (0.1, 0.5)$, $I \in (0^\circ, 25^\circ)$ and split them into a grid of $40 \times 40 \times 5$ boxes. With the aim to improve our statistics, we randomly generated two more test particles in the vicinity of each central particle (the dispersion of particles is not exceeding 20 per cent of the box size). In this way we created the initial conditions for 24 000 test particles.

In the next step, we integrated the orbits for $t_{\rm span} = 10$ Myr. For all these simulations, we use the symplectic integrator SWIFT (Levison & Duncan 1994) with a built-in second-order symplectic scheme (Laskar & Robutel 2001) and with an implementation of digital filters for the computation of the resonant elements based on criterion (4) (Brož et al. 2005). This symplectic integrator enables us to use a time step $\Delta t = 91.3125$ d. The simulations we perform are simplified: as we study the outer main belt we take into account only the gravitational interactions with the Sun and the four giant planets. The terrestrial planets are neglected, except for a barycentric correction applied to the initial conditions. We use the Laplace plane to define our initial frame of reference. We do not consider any non-gravitational acceleration at this point.

The final step was to calculate the distance d for each test particle. The average value $\bar{d}$ for the particles initially placed in the same box was taken as a measure of the dynamical instability in the box. Note that there is no temporal measure in this method, i.e. the map reflects the maximal displacement in each box during the integration time span $t_{\rm span}$ but it does not say how fast did this displacement occur.

We plot the mean values $\bar{d}$ in the top panel of Fig. 1 . The map is an average projection of all sections in $\sin I_{\rm r}$ to the ($a_{\rm r}$, $e_{\rm r}$) plane. It can be compared with several separatrices derived by Moons et al. (1998). It is clear that the map reflects the inner secular structure of the 2:1 resonance very well: we can locate both the stable islands A and B, separated by the ν_{16} secular resonance. The borderline at higher values of $e_{\rm r}$ is formed by the Kozai and ν_5 separatrices. The low-eccentricity region near the libration centre is affected by presence of multiple secondary resonances (Roig & Ferraz-Mello 1999).

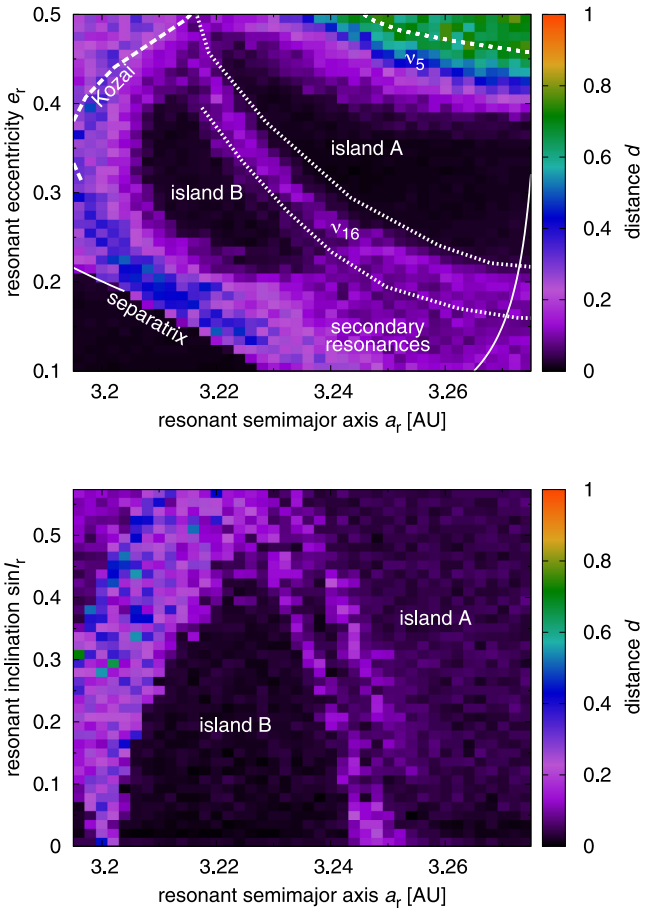

Figure 1. A dynamical map of the 2:1 mean-motion resonance with Jupiter computed in the present configuration of giant planets. Top panel: the map is plotted in the resonant semimajor axis a_r versus resonant eccentricity e_r plane and it is averaged over five sections in the resonant inclination $\sin I_r$. The colour coding of boxes represents the average distance in the phase space travelled by a test particle with initial orbital elements placed within the box. Additionally, separatrices and borders of the secular resonances, which were computed by Moons et al. (1998), are plotted over the map. The left solid line corresponds to the separatrix of the J2/1. The near-vertical solid line is the libration centre of the J2/1. The dotted lines indicate the ν_{16} and ν_5 resonance, and the dashed line represents the Kozai resonance. We mark the stable islands denoted A and B and also the region of overlapping secondary resonances (Roig & Ferraz-Mello 1999). Bottom panel: the map plotted in the resonant semimajor axis a_r versus sine of resonant inclination $\sin I_r$ plane. It was computed for test particles with the resonant eccentricity $e_r = 0.25$.

The bottom panel of Fig. 1 displays the projection of our map to the $(a_r, \sin I_r)$ plane but this time for a small interval of e_r because the shape of the separatrices and stable islands strongly depends on e_r. The map demonstrates how the shape of the stable islands changes with the resonant inclination I_r.

Let us conclude that the suitability of the resonant elements for the dynamical mapping serves as an independent confirmation that they indeed reflect the regularity of resonant orbits and they retain important properties of the proper elements at the same time.

2.3 Lifetimes of asteroids in the 2:1 resonance

Let us now discuss our approach to the identification and classification of the resonant asteroids. We numerically propagated the orbits of known numbered and multi-opposition asteroids in the broad surroundings of the J2/1 to identify those trapped inside, using a time series of the critical argument σ. We extracted the osculating elements of the main-belt objects from the AstOrb data base (Bowell 2012) as of 2012 November 15 to set-up the initial conditions for the first short-term integration. Our choice of the borders in the osculating (a, e) plane was $e_1 = 0.45(a - 3.24)/(3.1 - 3.24)$ and $e_2 = 0.5(a - 3.24)/(3.46 - 3.24)$. We ended up with 11 469 orbits. The corresponding planetary ephemeris were taken from JPL DE405 (Standish 2004) for the given Julian date. We numerically integrated the orbits for 10 kyr and we recorded the critical argument σ for each asteroid during the simulation. We have found 374 librating asteroids.

The following long-term integration requires a different approach. Our goal is to determine the future orbital evolution of the resonant asteroids and estimate their dynamical lifetime. However, we are limited by strong chaotic diffusion in the J2/1 resonance. In other words, even a slight change of the initial conditions can significantly alter the orbital evolution. Because the orbital elements of each observed asteroid are only known with a finite accuracy, one should consider all values within the observational uncertainty as possible initial conditions to cover all alternatives of future orbital evolution.

To account for this chaotic behaviour, we first matched the AstOrb data for librating asteroids with corresponding AstDyS uncertainties (Knežević & Milani 2003). The matching failed in four cases[1] only and hence we discarded these bodies from the J2/1 population. We then used a pseudo-random generator to create a bundle of 10 synthetic orbits for each asteroid which are close to its nominal orbit. The generated orbital elements fall within the Gaussian distribution (over $\pm 3\sigma$ interval) in the non-singular osculating element space. These synthetic test particles are called close clones. In this manner, we obtained 4070 orbits (1 nominal and 10 synthetic for each body) which we integrated over 1 Gyr. By this procedure, we can study several possible realizations of future orbital motion.

Following again Roig et al. (2002), we define the dynamical lifetime τ as the asteroid's time span of residence inside the resonance. Test particles leaving the resonance are usually discarded due to highly eccentric or inclined orbits, which lead to planetary crossing or fall into the Sun. We calculated the median dynamical lifetime $\bar{\tau}$ as the median value of the residence lifetimes of close clones.

We divided the J2/1 asteroids into three groups by virtue of their median dynamical lifetime $\bar{\tau}$ as follows:

(i) $\bar{\tau} \leq 70$ Myr: short-lived/unstable/Zulus. Number of identified bodies: 140.
(ii) $\bar{\tau} \in (70, 1000)$ Myr: long-lived/marginally stable/Griquas. Number of identified bodies: 106.
(iii) $\bar{\tau} \geq 1$ Gyr: long-lived/stable/Zhongguos. Number of identified bodies: 124.

For reference, the numbers of resonant asteroids identified in the previous paper Brož & Vokrouhlický (2008) were 92 short-lived and 182 long-lived asteroids.

We used the same long-term integration of the resonant orbits to construct orbital distribution of asteroids in the J2/1. We calculated average values of the resonant elements for each asteroid and each close clone over the time interval of 1 Myr; then we computed

[1] These particular bodies have the following designations: 2003 EO31, 2003 HH4, 2006 SE403 and 2006 UF152. The reason for the data bases mismatch might be in different methods used for orbit identification.

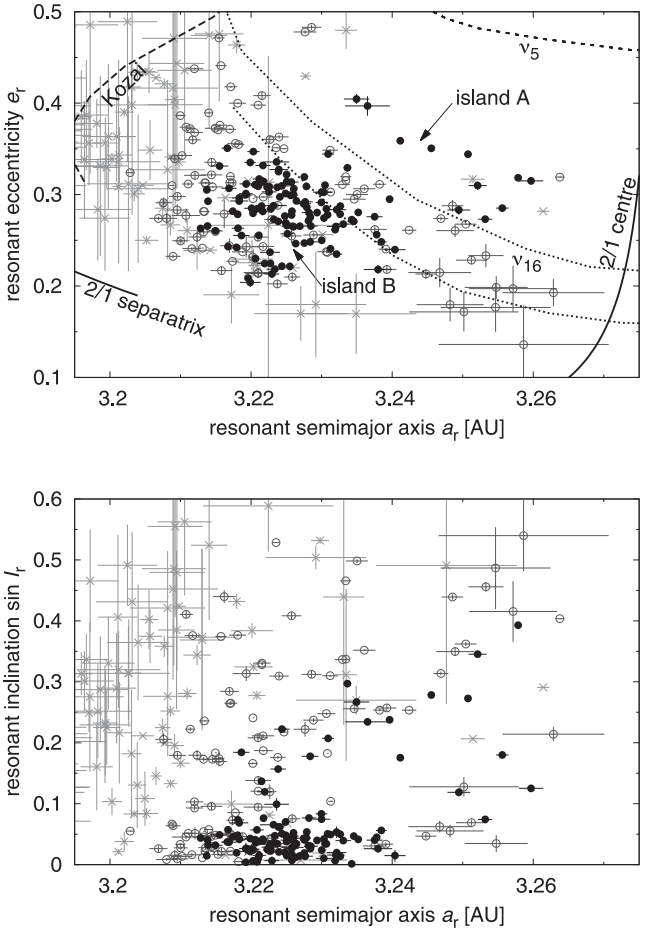

Figure 2. Orbital distribution of the J2/1 asteroids in the resonant semimajor axis a_r versus the resonant eccentricity e_r plane (top) and in a_r versus sine of the resonant inclination sin I_r plane (bottom). The symbols correspond to the dynamical lifetime of each body: filled circles denote dynamically stable Zhongguos, empty circles marginally stable Griquas, crosses unstable Zulus. The error bars indicate standard deviations of the computed orbits. We show the same borders and structures as in Fig. 1. Only a relatively small part of the unstable population is depicted.

the arithmetic mean for the asteroid and its close clones together. We define the standard deviation of the resonant elements as the uncertainty of the arithmetic mean.[2]

We depict the resulting mean resonant elements as projections to the (a_r, e_r) and (a_r, sin I_r) planes in Fig. 2. The orbital distribution exhibits similar properties as in the previous studies. Zhongguos reside at the very centre of the stable islands, 11 Zhongguos in island A and 113 in island B. The majority of B-island Zhongguos have low-resonant inclinations while A-island Zhongguos are more inclined. Griquas partially overlap with the Zhongguo group, but they either reside on orbits with lower semimajor axis or higher inclination than Zhongguos. There is no clear separation between the orbits of Griquas and Zhongguos. It is therefore questionable whether the division of the long-lived population into these two

[2] Let us note that the standard deviations of the mean resonant elements will be slightly overestimated. The reason for this arises from our approach to the generation of initial conditions because the initial elements of the close clones are generated *randomly* thus resulting in uncorrelated sets of quantities even though they should be correlated, as described by the correlation matrices available in orbital elements data bases.

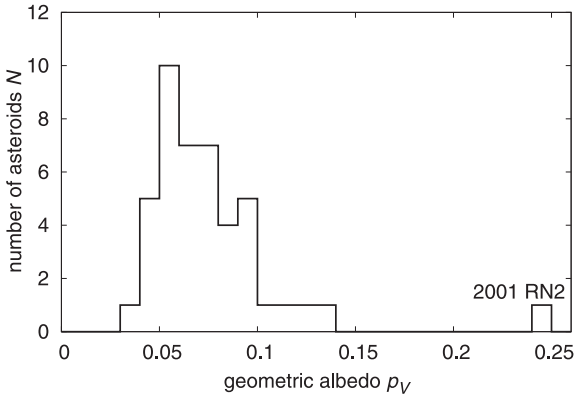

Figure 3. A histogram of the albedo distribution among the J2/1 asteroids: the visual geometric albedo p_V versus the number of asteroids N. The data for 44 asteroids were available in Masiero et al. (2011).

groups has a solid physical foundation, apart from the dynamical lifetime. The orbital position of Griquas with respect to Zhongguos indicates that Griquas might be chaotically diffusing part of Zhongguos which have haphazardly entered the periphery regions of the stable islands.

Since we focus on the long-lived population, a great part of the short-lived bodies is not displayed in Fig. 2 (they are located outside the range of the plot). The depicted short-lived asteroids are chaotically drifting towards the Kozai separatrix.

2.4 Albedo, colour and size–frequency distributions

In order to study the basic physical properties of the J2/1 population, we first searched the WISE data base. We were able to extract the visual geometric albedos p_V and the effective diameters D, inferred from NEATM thermal models by Masiero et al. (2011), for 44 asteroids inside the J2/1 (out of 370).

The data obtained allow us to examine the albedo distribution in the resonance (Fig. 3). The lowest albedo is (0.034 ± 0.002) while the largest value is (0.24 ± 0.03). This relatively large value corresponds to asteroid 2001 RN2 and indicates that this object likely belongs to the S taxonomic type. The majority of the asteroids (98 per cent) have albedo lower or equal to (0.136 ± 0.004). The shape of the albedo distribution is typical for the outer main-belt region where C-types dominate (e.g. DeMeo & Carry 2013).

As the next step, we investigated the diameters of asteroids. For the 44 cases we simply use the value D and its uncertainty. For the rest of the asteroids we calculate their approximate diameter using the following relation (Harris 1998):

$$D = \frac{1329}{\sqrt{p_V}} 10^{-\frac{H}{5}}, \quad (6)$$

where we insert the absolute magnitude H from the AstOrb catalogue and we use the mean albedo $\bar{p}_V = (0.08 \pm 0.03)$. The standard deviation of D is then computed as the propagated uncertainty of both H and $\bar{p}_V$.

We construct the cumulative SFDs of the resonant population and individual groups, as shown in Fig. 4. We fit the steep part of the distribution with a power-law function $N(>D) \propto D^{\gamma}$ to estimate the slope parameter γ for further comparison. The value of γ clearly depends on the chosen interval of diameters over which we approximate the SFDs with the power law. We set the nominal fitted interval as $D \in (7.5, 18)$ km. The SFDs start to bend at the lower limit of this nominal interval except for SFD of Griquas which remains steep up

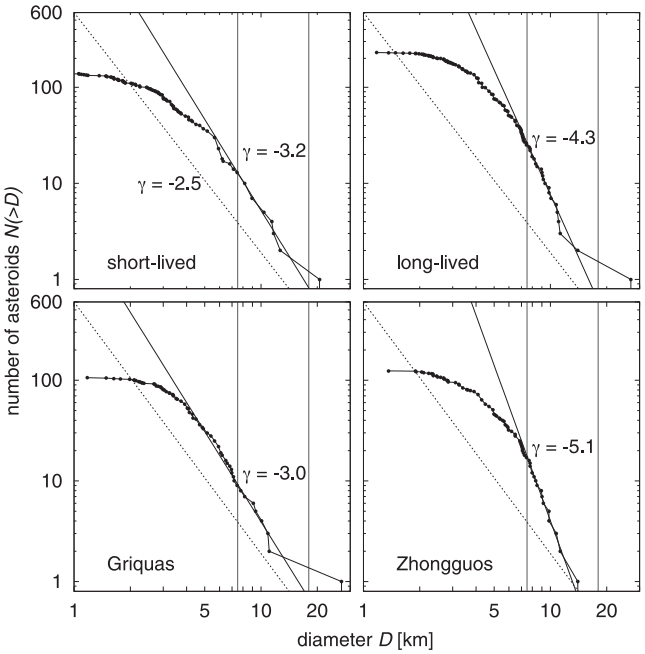

Figure 4. SFDs of individual dynamical groups residing inside the J2/1: the diameter D versus the cumulative number $N(>D)$ of asteroids larger than D. A logarithmic scaling is used in the plot. The distributions correspond to the short-lived population (top left) and long-lived population (top right), which is then divided to marginally stable Griquas (bottom left) and stable Zhongguos (bottom right). The steep part of each distribution is approximated with a power-law $N(>D) \propto D^{\gamma}$. The nominal borders of the fitted regions (ranging from 7.5 to 18 km) are shown by vertical lines. The value of the slope γ is also given. We also plot stationary Dohnanyi-like slope ($\gamma = -2.5$) for comparison.

Table 1. The slopes γ resulting from the method of least squares which we applied to fit the SFDs of dynamical groups with a power-law function $N(>D) \propto D^{\gamma}$. The middle column shows the result of the fit in the nominal interval of diameters $D \in (7.5, 18)$ km, the third column reflects the variation of γ if the limits of the interval are shifted.

Group	Nominal γ	Variation of γ
Short-lived	−3.2	(− 2.5, −3.7)
Long-lived	−4.3	(− 3.7, −5.1)
Griquas	−3.0	(− 3.0, −3.3)
Zhongguos	−5.1	(− 3.9, −5.1)

to $D \simeq 4$ km. We also record the variation of the slope γ by slightly changing the fitted range of diameters. The results are summarized in Table 1. Unlike the results of Brož et al. (2005), the SFD of updated Griquas is not shallower than a Dohnanyi-like SFD with $\gamma = -2.5$ (Dohnanyi 1969). In Section 5, we shall use the observed SFDs for comparison with the outcomes of our collisional models.

Finally, we also searched the SDSS MOC catalogue (Parker et al. 2008). We found astrometric and photometric data for 81 resonant bodies for which we constructed a colour–colour diagram (see Fig. 5). The principal component denoted as $a^{\star}$ is defined on the basis of measurements in filters r, i and g as $a^{\star} = 0.89(g - r) + 0.45(r - i) - 0.57$ and it can be used to distinguish C-complex ($a^{\star} < 0$) and S-complex ($a^{\star} > 0$) asteroids. The distribution in the diagram

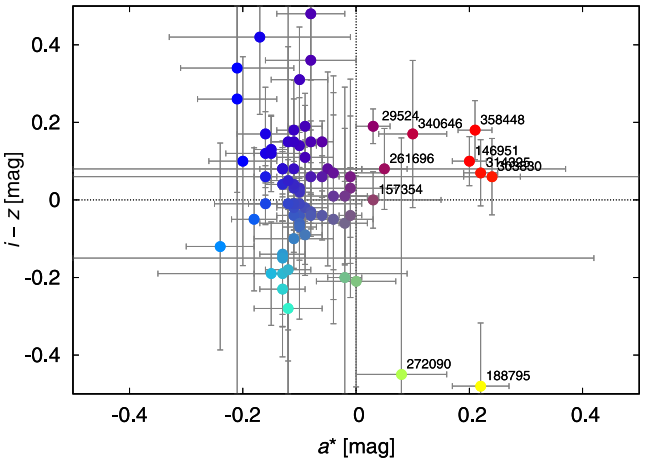

Figure 5. The optimized colour $a^{\star}$ versus the $i - z$ colour diagram of the J2/1 resonant asteroids found in the SDSS MOC catalogue. Error bars represent the standard deviations of the displayed quantities. The outliers with $a^{\star} > 0$ are labelled with corresponding catalogue numbers.

is typical for outer main-belt C-type asteroids, but one can also see several outliers with $a^{\star} > 0$. We did not find any significant relation between the colours and the orbital distribution.

2.5 The long-term stability of the islands A and B

The observed resonant population has likely evolved over Gyr-long time-scales. Hence, it is important to assess its dynamical stability over similarly long time spans. This problem was recently revisited by Skoulidou, Tsiganis & Varvoglis (2014). Here we will use the main results of this study that are relevant for our work; a complete dynamical study will be presented in a different paper (Skoulidou et al., in preparation).

When studying the outer asteroid belt, we typically ignore the weak perturbative effects of the terrestrial planets, as this speeds up the numerical propagation. Skoulidou et al. (2014) showed that this is not a safe option, when studying the 2:1 resonant population for time spans longer than 1 Gyr, as numerous weak encounters with Mars actually induce small-scale chaotic variations. These variations build-up slowly with time and eventually assist in breaking the phase-protection mechanism that would otherwise prevent asteroids on moderately eccentric orbits ($e \sim 0.4$) from encountering Jupiter on this time span. Moreover, when the Yarkovsky effect is added, asteroids with $D < 20$ km can escape from the resonance more efficiently. This is because, as also shown in Brož & Vokrouhlický (2008), the combined action of resonance and slow Yarkovsky drift forces the asteroid orbits to slowly develop higher eccentricities as a consequence of adiabatic invariance. The computations presented in Skoulidou et al. (2014) show that, in a physical model that takes into account the aforementioned phenomena, the 2:1 population would decay roughly exponentially in time, with an e-folding time of order 1 Gyr.

In Fig. 6 we present the results of a similar simulation that spanned 3 Gyr, in a model that contained the seven major planets (Venus to Neptune; '7pl' model). This simulation treated the 2:1 population, as was defined by Brož & Vokrouhlický (2008). Also, an approximate treatment of the Yarkovsky acceleration was included in the equations of motion, assuming a constant drift rate in semimajor axis equal to $2.7 \times 10^{-4} D^{-1}$ au Myr^{-1}. For each object its diameter D was estimated, using its catalogued H value and assuming an albedo of 0.06–0.08, and a value of either 0° or 180° obliquity

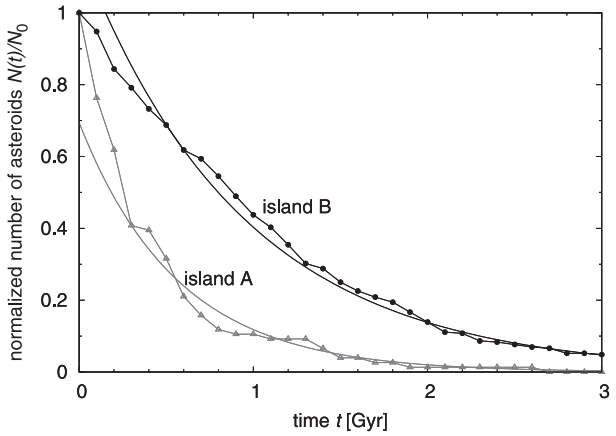

Figure 6. Time evolution of the number of resonant objects, $(N(t)/N_0)$, normalized to the initial value. This is the result of a 3-Gyr-long simulation, within the framework of the 7-planets model and including Yarkovsky-induced drift in a. The two curves refer to the two islands (A=open triangles and B=filled circles). Superimposed are the least-squares fitted exponentials, yielding e-folding times of $\tau_A = (0.57 \pm 0.02)$ Gyr and $\tau_B = (0.94 \pm 0.02)$ Gyr, respectively.

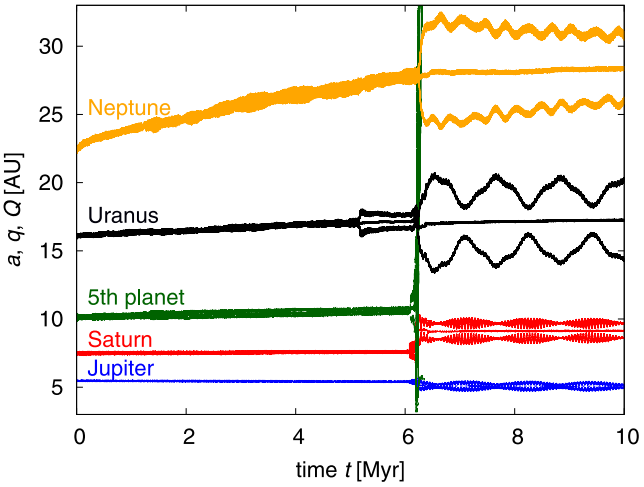

Figure 7. Orbital evolution of giant planets in the fifth giant planet scenario, adopted from Nesvorný & Morbidelli (2012), during the jumping-Jupiter instability, as it was reproduced by our modified integrator. We plot the time t versus the semimajor axis a, the pericentre q and the apocentre Q. Each evolutionary track is labelled with the name of the corresponding giant planet.

was randomly assigned. The population was found to decay exponentially in time, according to what was described in the previous paragraph.

However, what is more interesting here is that the two subpopulations that are contained in the two quasi-stable resonant islands are not diffusing out at the same rate. Fig. 6 shows two sets of curves (one for each island): clearly island A is depleted faster than island B. Fitting exponentials on the data, we get the corresponding e-folding times: $\tau_A = (0.57 \pm 0.02)$ Gyr for island A and $\tau_B = (0.94 \pm 0.02)$ Gyr for island B. This uneven depletion is an important dynamical property of the resonance and is likely one of the reasons behind the observed A/B asymmetry. The importance of this observation will become more evident in the following sections.

3 EFFECTS OF THE JUMPING-JUPITER INSTABILITY

We investigate the role of the jumping-Jupiter instability on the depletion and eventual repopulation of the J2/1 in this section. We study survival of a hypothetical primordial population, and resonant capture from the outer main belt, both in the fifth giant planet scenario (Nesvorný & Morbidelli 2012). Our simulations cover only the instability phase itself, demonstrating at first which process is plausible.

3.1 Simulations with prescribed migration

We adopt the technique suggested by Nesvorný et al. (2013) for simulating the jumping-Jupiter instability. We modified the SWIFT_RMVS3 integrator (Levison & Duncan 1994), so that the evolution of massive bodies is given by a prescribed input file and the evolution of test particles is computed by the standard symplectic algorithm. This method allows us to exclude the trans-Neptunian disc of planetesimals from our integrations, because its damping and scattering effects are no longer needed; planets evolve 'the way they are told' by the input file. Moreover, the exact progress of the migration scenario is then exactly reproducible.

The evolution of migrating planets is prescribed by the fifth giant planet scenario, developed in Nesvorný & Morbidelli 2012 (see Fig. 7). This scenario has already been proven reliable in terms of reproducing the orbital architecture of planetary orbits, the period ratios and secular frequencies, and several distributions of minor Solar-system bodies. The prescribed input file is the result of a complete self-consistent simulation with five giant planets and a massive trans-Neptunian disc of planetesimals ($M_{\rm disc} = 20\,M_{\rm Earth}$). We use only a 10 Myr portion of the simulation, containing the jumping-Jupiter phase. The input data sampling is $\Delta t_{\rm input} = 1$ yr which is sufficient for our purpose.

Our integrator transforms the input data to the Cartesian coordinates (i.e. orbital elements to positions and velocities) and interpolates them according to the integration time step $\Delta t = 0.25$ yr. The interpolation is done by a forward/backward drift along Keplerian ellipses, starting at input data point preceding/forthcoming to required time value. The results of both drifts are averaged using the weighted mean, where the weight depends on temporal distance between the data points and the required time value.

3.2 Capture from the outer main belt

We investigated a possibility that the resonant asteroids were captured from outer main-belt orbits near the J2/1 during Jupiter's jump. We present a simulation of the capture in this section.

Initial conditions: Initially, we distributed 5000 test particles uniformly over the region which is about to be covered by the moving 2:1 resonance. This can be estimated easily by Kepler's third law since we know the evolution of Jupiter's semimajor axis a priori. Our choice of the semimajor axes distribution was $a \in (3.06, 3.32)$ au. The distribution of eccentricities and inclinations was also chosen as uniform and corresponds to the extent of a moderately excited main belt: $e \in (0, 0.35)$, $I \in (0^\circ, 15^\circ)$. The angular elements were randomly distributed over $(0^\circ, 360^\circ)$ interval.

Evolution of test particles: We recorded the time series of resonant elements of the test particles during the integration and processed them off-line using the Savitzky–Golay smoothing filter (Press et al. 2007) with 0.1 Myr range of the running window and a second-order smoothing polynomial.

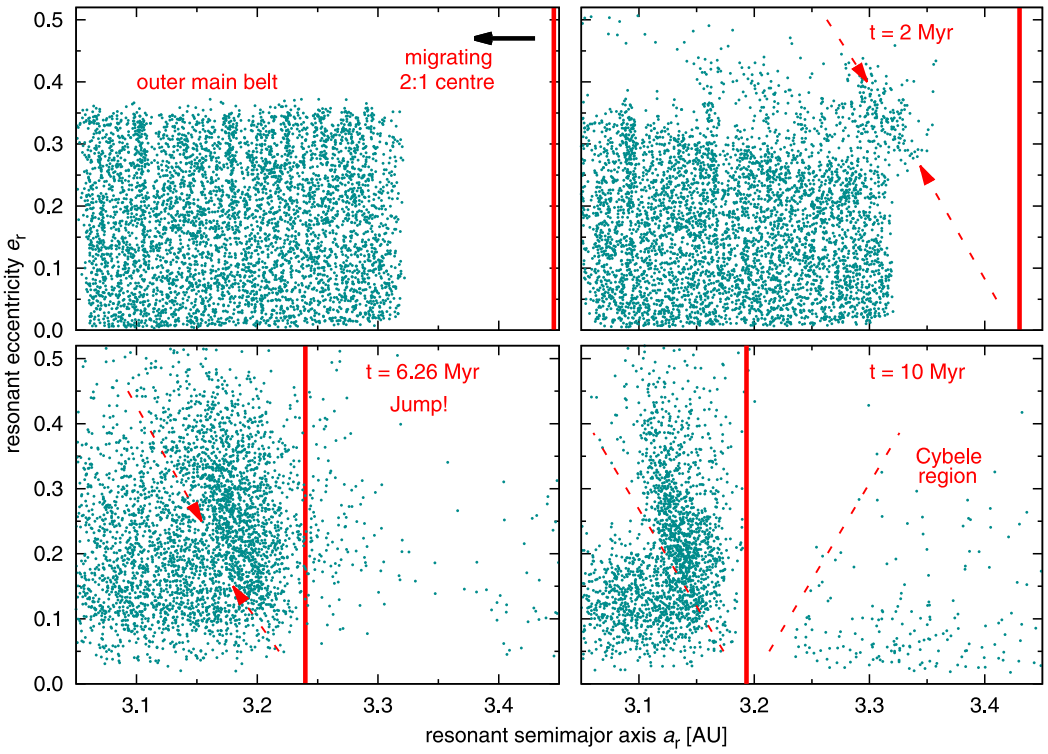

Figure 8. A simulation of the resonant capture from the outer main belt in the fifth giant planet scenario (Nesvorný & Morbidelli 2012). We plot the evolution of test particles in the resonant semimajor axis a_r versus resonant eccentricity e_r plane. The vertical line indicates an approximate location of the 2:1 resonance centre which migrates inwards together with Jupiter. The integration time is shown in three of the panels (t = 0, 2, 6.26 and 10 Myr) and corresponds to the time-line in Fig. 7. The dashed arrows and lines indicate an approximate extent of the libration zone in the case of the migrating and stable resonance, respectively. From top to bottom and left to right, the plots show: the initial conditions, the relaxed population of test particles prior to jump, the state during the jumping-Jupiter instability and the final state. Note that all test particles are depicted in terms of resonant elements for simplicity (even the non-resonant orbits).

The result of our simulation is shown in Fig. 8. Note that for the sake of simplicity, we use the resonant elements for *all* particles, even for those not trapped inside the J2/1.[3] Shortly after the onset of migration, the test particles still retain the uniform character of the initial distribution. A few minor mean-motion resonances can be identified. The apparent gap between the resonance centre and the synthetic population is intentional, because we do not want any of the test particles to be initially placed inside the resonance.

After 2 Myr, the relaxation processes start to take place. The 2:1 resonance changes its position with respect to the initial one and starts to perturb several eccentric orbits at the outskirts of the synthetic population. All of the perturbed asteroids fall into the short-lived unstable zone (discussed in Brož et al. 2005). The minor mean-motion resonances begin to pump the eccentricity of the test particles residing inside them.

At 6.26 Myr, an instantaneous discontinuity, known as *Jupiter's jump*, occurs. The 2:1 resonance, comoving with jumping Jupiter, changes its location suddenly and a large number of test particles flow through the libration zone, while others are excited and ejected, or left behind in the emerging inner Cybele region.

Finally at 10 Myr, a population between the left-hand separatrix and the libration centre is stabilized, as the result of the resonant capture. The bodies outside the left-hand separatrix are simply remnants of the initial population of test particles. A few bodies between the libration centre and the right-hand separatrix are in fact outside the 2:1 resonance, as well as the asteroids in the Cybele region.

Captured population: Instead of another long-term integration, we use the rather efficient dynamical mapping introduced in Section 2.2 to check the stability of the captured population in the post-migration configuration of planets. This allows us to identify the counterparts of the stable islands A and B in the phase space for this planetary configuration. Hence, we can trace the long-lived candidates of our captured bodies simply by selecting particles with resonant elements falling within the range of the islands.

The dynamical map for the 2:1 resonance is shown in the Fig. 9. It covers the phase space in the intervals $a \in (3.115, 3.195)$ au, $e \in (0.1, 0.5)$ and $I \in (0°, 25°)$, which were divided into a grid of $40 \times 40 \times 5$ boxes (and we finally took an average over all sections in the inclination). We set up and followed three test particles per box for up to 10 Myr.

Comparing the map with Fig. 1, one can see very similar structures. The stable islands A and B are there, separated by the ν_{16} secular resonance. The Kozai resonance separatrix can also be easily identified. A major difference is the shape and size of the A island – the ν_5 resonance is not present in the depicted part of the phase space, which effectively enlarges the A island with respect to the present state. The selected candidates for long-lived orbits are also shown in Fig. 9. Note that there are very few A-island bodies captured on highly eccentric orbits, therefore the aforementioned difference in shape of island A should not strongly affect the results.

[3] The resonant elements of the non-resonant asteroids do not have any special physical meaning, but they correspond to the extremal secular variations of osculating elements as given by equation (4).

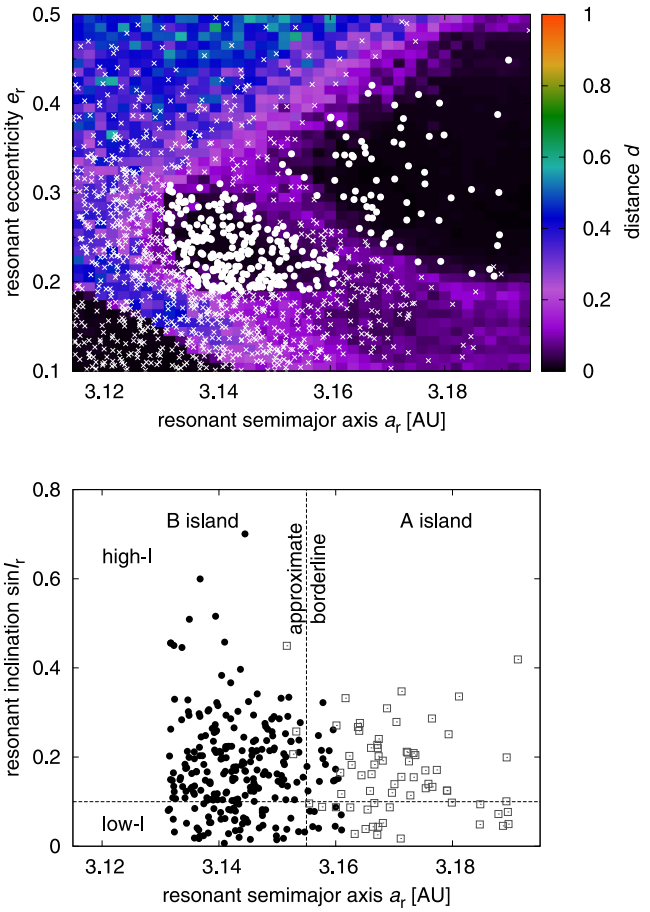

Figure 9. A final result of resonant capture from the outer main belt in the fifth giant planet scenario. Top: the resonant semimajor axis a_r versus the resonant eccentricity e_r. The background of the plot is the dynamical map of the 2:1 mean-motion resonance with Jupiter computed for the post-migration configuration of the giant planets. All white symbols indicate orbits of test particles captured during the simulation (they correspond to the final state in Fig. 8, but only a part of the phase space containing the stable islands is plotted). Test particles embedded in the dark regions of the dynamical map are candidates for a long-term stability and we distinguish them by circles. Other particles are marked by crosses. Bottom: the resonant semimajor axis a_r versus sine of the resonant inclination $\sin I_r$. We plot only the particles captured inside the stable islands. Black circles indicate test particles captured in island B and grey open squares indicate those captured in A island. The horizontal dashed line is plotted for reference, because vast majority of the observed B-island Zhongguos reside on low inclinations $\sin I_r \leq 0.1$ and all of the observed A-island Zhongguos have high inclinations $\sin I_r \geq 0.1$.

Using the dynamical mapping, we identified $N_A^{synth} = 69$ candidates in island A and $N_B^{synth} = 254$ candidates in island B.

The next step is a rescaling of the initial population so its particle density would reach realistic values. We used the observed particle density in the main belt for bodies with diameters $D \geq 5$ km within the following region: $a \in (2.95, 3.21)$ au, $e \in (0, 0.35)$, $I \in (0^\circ, 15^\circ)$. The intervals of e and I correspond to those of our synthetic initial population. On the other hand, the interval of semimajor axes was shifted into the region which is currently not depleted by the presence of the J2/1. We further increased this particle density by a factor of 3 (Minton & Malhotra 2010) to account for the dynamical depletion of the main belt after the reconfiguration of planets during the last $\simeq 3.85$ Gyr. If we increase the particle density throughout the initial population, the number of captured long-lived bodies larger than 5 km would be $N_A^{scaled} = 1552$ and $N_B^{scaled} = 5857$ in island A and B, respectively.

Finally, we assume that the dynamical depletion rate due to chaotic diffusion is the same for the post-migration islands as for the islands in the observed configuration. Knowing the approximate number of captured long-lived asteroids, we employ an exponential decay law and the extremal values[4] of the e-folding times in island A and B: $\tau_A = (0.57 \pm 0.05)$ Gyr and $\tau_B = (0.94 \pm 0.05)$ Gyr. We use $t = (3.9 \pm 0.1)$ Gyr as a value of the decay time period. Combining the results together and identifying the limit values, our model predicts that we should observe $N_A^{model} = 1$–3 long-lived bodies larger than 5 km in island A and $N_B^{model} = 62$–121 asteroids in island B. The observed values are $N_A^{obs} = 2$ and $N_B^{obs} = 71$. The results of our model and the observed values are in good agreement, which supports the resonant capture scenario.

Turning our attention to the bottom panel in Fig. 9, we can discuss whether the inclination distribution of captured synthetic bodies can evolve towards the observed one. It can be clearly seen that the number of low-I asteroids in island A is lower than the number of high-I asteroids. Assuming strong depletion of the whole island and considering that only 1–3 objects larger than 5 km may survive up to the present according to our model, the low-I asteroids are more likely to be depleted completely. That is in agreement with the observations because the observed asteroids in island A reside exclusively on highly inclined orbits.

On the other hand, the population captured in island B stretches almost uniformly over a relatively large interval of inclinations. Considering the shape of the real island shown in Fig. 1, which shrinks with increasing inclination, the long-term diffusion in the high-I region will partially deplete this part of the captured population. But in order to reproduce the observed state in island B, it is necessary for the source population to contain low-I asteroids predominantly.

3.3 Survival of the primordial population

Let us study hypothetical long-lived primordial orbits and their survival during the planetary migration. The procedure is similar to that in the previous section, the major difference is of course in the initial conditions set-up. Here we aim to study only the bodies which reside inside the J2/1 when the instability simulation begins. Another important property that should be satisfied is the long-term stability of the initial orbits – otherwise one could unintentionally simulate different effects such as survival of the short-lived population, etc.

Initial conditions: How to create a set of test particles on the long-lived orbits at the beginning of the migration scenario? The only viable solution is to use the dynamical mapping once again. To this effect, we slightly modify the standard procedure described in Section 2.2. First, the integration is not done in a stable unvarying configuration of planets. It is instead carried out during the first 5 Myr of the prescribed migration scenario, starting in the pre-

[4] These values were derived in Section 2.5 but we use a slightly higher standard deviation (0.05 instead of 0.02). The reason is that the e-folding times were obtained from a model with seven planets and the Yarkovsky drift included, with long-lived asteroids of *all* sizes. In this section, however, we focus on asteroids larger than 5 km and consequently, the e-folding times are rather upper limits for us. We thus artificially increase the original deviation to account for this difference.

migration configuration of planets and evolving into a configuration closely preceding the instability.

Secondly, we use only the recorded changes of the resonant inclination $\delta \sin I_\mathrm{r}$ when constructing the map [i.e. we omit δa_r and δe_r when evaluating the metric given by equation (5)]. This is necessary because as Jupiter migrates inwards, the resonance follows and the resonant semimajor axis a_r of bodies residing inside decreases. This in turn changes the resonant eccentricity e_r because of the adiabatic invariance of resonant orbits. These changes are systematic and have different amplitudes for different orbits. Consequently, they should not be incorporated when calculating the distance d. On the other hand, our numerical runs suggest that the resonant inclination I_r of test particles does not undergo substantial systematic changes under the influence of migrating giant planets. If a large change in inclination is registered, it usually means that a secular resonance affected the orbit. The resulting dynamical map thus represents what we need – the location of regions crossed by secular resonances and the stable islands lying in between for the time period before Jupiter's jump.

Our choice of boundaries in the phase space to construct the dynamical map was $a \in (3.32, 3.45)$ au and $e \in (0, 0.6)$. We created 40×40 grid in the (a, e) plane and covered it uniformly with six particles per each cell, assigning a fixed value of $I = 2.5^\circ$ to all of them. As already mentioned, the planetary migration is not able to strongly change the inclinations, that is why we map the region of low inclinations where the observed long-lived population dominates. The resulting pre-instability dynamical map is displayed in Fig. 10.

We randomly distributed a group of 2000 test particles over the identified stable islands (see Fig. 11) with low inclinations $I < 5^\circ$

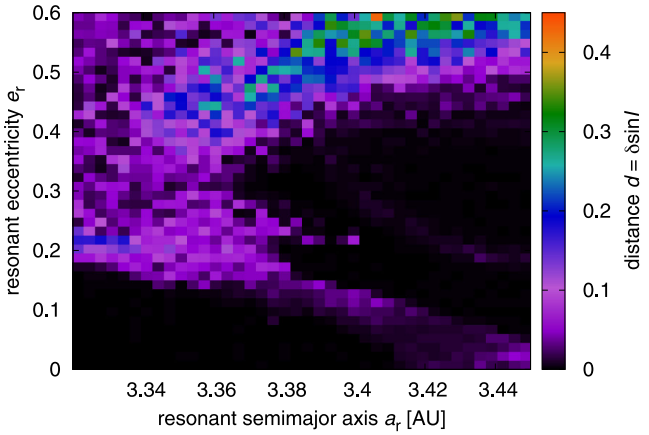

Figure 10. A dynamical map of the 2:1 mean-motion resonance with Jupiter computed during the pre-instability evolution of giant planets. The map is displayed in the resonant $(a_\mathrm{r}, e_\mathrm{r})$ plane corresponding to $I_\mathrm{r} = 2.5^\circ$. Note that only the displacement in the resonant inclination δI_r is used to represent the dynamical stability.

to set up a synthetic primordial population for our simulation. The angular osculating elements were chosen in such a way that condition (3) holds and the osculating elements are therefore identical to the resonant elements at $t = 0$.

Evolution of test particles: 2 Myr after the onset of the migration, the orbits are not significantly dispersed which is in agreement with our aim to study only the dynamically stable resonant bodies. After 6.1 Myr, the close encounters of giant planets begin to occur and start

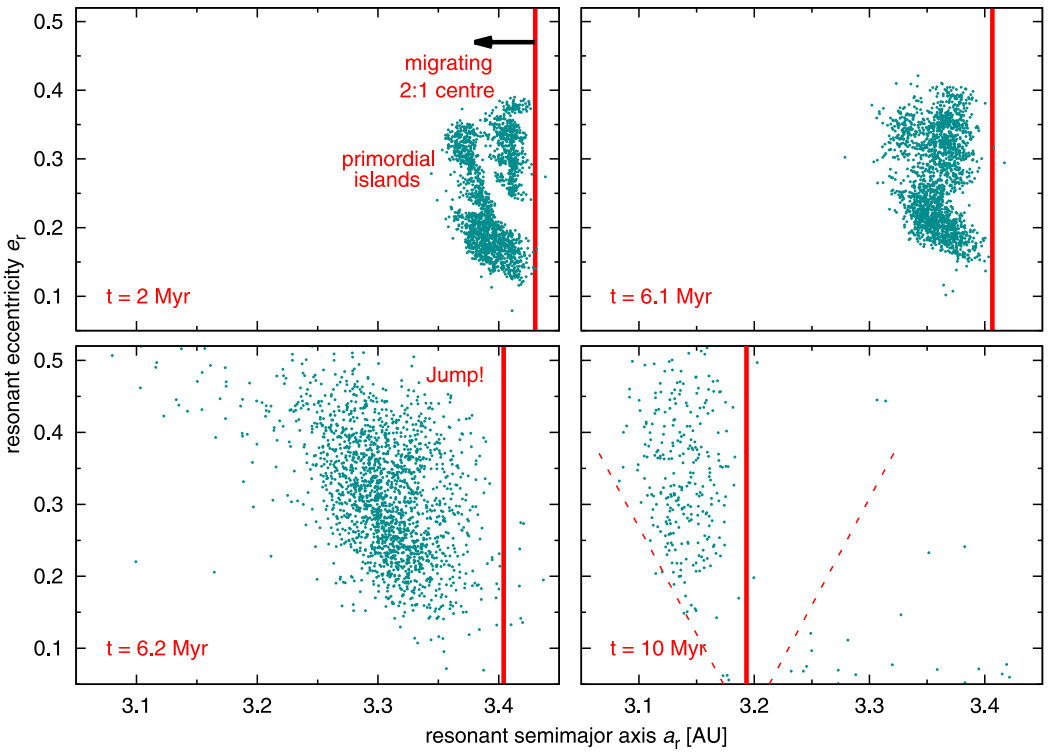

Figure 11. A simulation of the primordial population survival in the fifth giant planet scenario (Nesvorný & Morbidelli 2012). The evolution of primordial long-lived orbits in the $(a_\mathrm{r}, e_\mathrm{r})$ plane is displayed. The vertical line indicates the migrating 2:1 resonance. The initial population was placed inside the islands identified in Fig. 10, top-left panel represents its orbital distribution 2 Myr after the onset of the migration. The following panels show the situation during Jupiter's jump and also the final state.

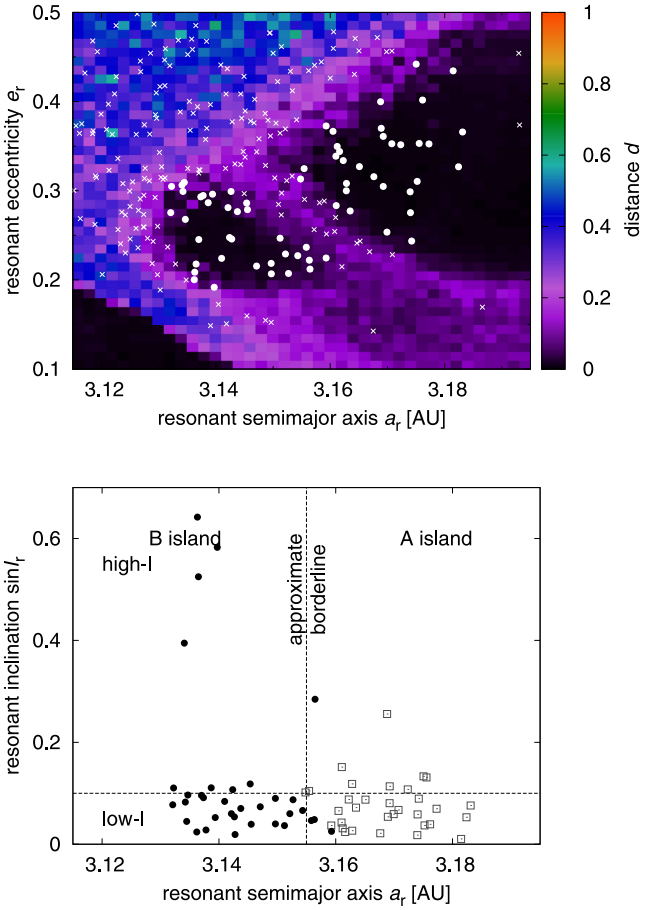

Figure 12. Top: the same post-migration dynamical map as in Fig. 9. The primordial test particles surviving the jumping-Jupiter instability are plotted over the map. Circles represent candidates for long-lived orbits and crosses are the surrounding orbits. Bottom: the resonant semimajor axis a_r versus sine of the resonant inclination sin I_r. We plot only the particles identified above as long-lived. Black circles indicate those residing in the island B and grey open squares indicate those residing in the A island.

to perturb the islands inside the J2/1. Progression of Jupiter's jump partially destabilizes the islands and enables significant number of bodies to leak out and also to populate other regions of the 2:1 resonance. At the end of migration, 85 per cent of the initial population is lost and the rest is dispersed all over the resonant region, except for the low-eccentricity region. This indicates that the only possible change in resonant eccentricity during the migration of Jupiter is to increase.

Surviving population: Following our procedure from Section 3.2, we used the same dynamical map to identify the long-lived asteroids (see Fig. 12) and we applied the rescaling and the long-term dynamical decay. Because the particle density in a hypothetical primordial population is not known, we varied the number of initial synthetic long-lived particles and calculated the expected number of asteroids in islands A and B surviving up to the present.

The selected results are listed in Table 2 and the comparison is made for asteroids with $D \geq 5$ km (we remind the reader that there are $N_A^{obs} = 2$ and $N_B^{obs} = 71$ larger than 5 km in the observed population). If we assume the particle density from Minton & Malhotra (2010), which we also used in Section 3.2, the contribution of the primordial asteroids to the observed population is negligible after long-term dynamical evolution.

Table 2. The numbers N_A^{model} and N_B^{model} of the asteroids surviving in the islands A and B up to the present as predicted by our model of the primordial population survival. The table represents how the resulting population changes with increasing number N_{init} of initial primordial asteroids. The bodies with $D \geq 5$ km are considered. First line roughly corresponds to the primordial population with particle density of the present outer main belt, the next two cases approximately consider the particle density proposed in Minton & Malhotra (2010). In the last line, we assume particle density of primordial main belt shortly after its creation, as suggested by Morbidelli et al. (2009); we note that this case is not very probable.

$N_{init}(D \geq 5$ km)	N_A^{model}	N_B^{model}
2000	0	0–1
5000	0	1–2
10 000	0	2–4
100 000	1–3	18–35

In order to observe a substantial contribution, the particle density in the J2/1 would have to be considerably larger than in the neighbouring main belt (at least ten times larger). Such particle density gradient is not very probable, because the 2:1 resonance would have to be dynamically protected against depleting mechanisms and perturbations, arising e.g. from planetary embryos (O'Brien, Morbidelli & Bottke 2007) or due to the compact primordial configuration of planetary orbits (Masset & Snellgrove 2001).

We also investigated if A-island orbits can become B-island and vice versa. We found that <1 per cent of the asteroids initially placed inside island A survive there and 1 per cent drift into B island during the migration. On the other hand, the primordial population of island B preserves 2 per cent of the original bodies and 2 per cent of them populate island A. Because the primordial B island is larger than the A island, it harbours more primordial asteroids under the assumption of homogeneous particle density. The contribution of island B to the surviving long-lived population therefore dominates. Also note that after the migration the ratio $N_A/N_B \simeq 1$, thus the migration itself is not able to create an asymmetric population out of surviving primordial asteroids. Further orbital evolution is needed in this case.

The orbital distribution in the (a_r, I_r) plane at the end of the planetary migration indeed resembles the initial interval of inclinations, as both islands are populated by low-I orbits. To obtain high-I orbits, which are observed in island A, we would have to assume the presence of their analogues in the pre-migration islands. But this problem is redundant since the primordial population probably do not survive up to the present, as we argued above.

4 EFFECTS OF JUPITER–SATURN GREAT INEQUALITY

In Section 3, we investigated evolution of the resonant population during a major instability of the planetary system known as Jupiter's jump. In the original migration experiments performed in Nesvorný & Morbidelli (2012), the violent evolution of planetary orbits was usually followed by a residual smooth migration during which giant planets slowly approached their current orbits. We are in a similar situation, the planetary configuration at the end of our instability simulations slightly differs from the observed one. In principle, this fact does not affect our ability to locate and describe the long-lived

resonant population of test particles because we employed fast and efficient method of dynamical mapping. The natural question then arises, whether the late migration stages can invoke perturbations that would affect the overall stability of the 2:1 resonance significantly.

In particular, we want to check whether the period P_σ of libration of the resonant asteroids can be comparable with the Jupiter–Saturn GI period $P_{\rm GI}$ (which is the period of circulation of the $2\lambda_{\rm J} - 5\lambda_{\rm S}$ angle) and what effect would it have on the resonant population (Ferraz-Mello et al. 1998, see also Section 1).

In order to mimic the smooth late planetary migration and lead giant planets towards their current orbits, we used a modified version of the SWIFT_RMVS3 integrator developed in Brož et al. (2011). The integrator introduces an ad hoc dissipation term which modifies planetary velocity vectors $\boldsymbol{v}$ in each time step Δt according to the following relation:

$$\boldsymbol{v}\,(t+\Delta t) = \boldsymbol{v}\,(t)\left[1 + \frac{\Delta v}{v}\frac{\Delta t}{\tau_{\rm mig}}\exp\left(-\frac{t-t_0}{\tau_{\rm mig}}\right)\right], \qquad (7)$$

where $\Delta v = \sqrt{GM/a_{\rm init}} - \sqrt{GM/a_{\rm fin}}$ is the total dissipation determined as the difference of the initial and final mean velocity, $\tau_{\rm mig}$ is the migration time-scale, t is the time variable and t_0 is an arbitrary initial time. The eccentricity damping is also included and can be set independently for each planet by choosing the damping parameter denoted as $e_{\rm damp}$ (Morbidelli et al. 2010).

To set up the model, we used the final configuration of giant planets and test particles from our simulations of resonant capture,[5] but we only selected test particles located in broader surroundings of the stable islands to discard major part of short-lived asteroids. After this procedure, we launched a set of integrations with different values of $e_{\rm damp}$ and different migration time-scales, bearing in mind that the time-scale of the original experiments in Nesvorný & Morbidelli (2012) was $\tau_{\rm mig} \simeq 30$ Myr. When the integrations finished, we selected only the runs in which giant planets ended up with orbital parameters similar to the observed ones and we investigated the results at the time $t_{\rm fin}$ when $P_{\rm GI} = 880$ yr and the ratio of the Saturn's and Jupiter's orbital periods is approximately $P_{\rm S}/P_{\rm J} \simeq 2.49$.

In the following, we will discuss results of two runs with $t_{\rm fin} \simeq 27$ and $\simeq 58$ Myr. Fig. 13 shows the temporal evolution of the number N of test particles in these two runs, the GI period $P_{\rm GI}$ and the libration period P_σ of two typical resonant asteroids. While P_σ oscillates around a nearly constant value $\simeq 420$ yr, $P_{\rm GI}$ initially lies below this value and rises smoothly as Jupiter and Saturn undergo divergent migration, and their eccentricities are damped.

The evolution of the $N(t)$ curves does not follow any simple decay law. This may serve as a proof that the level of chaotic diffusion inside the islands indeed evolves during the smooth late migration. The steepest slope of the $N(t)$ dependency is reached during the time interval when $P_{\rm GI} \simeq P_\sigma$. But one can also notice that the slope changes are smooth rather than sharp; the destabilization is not strictly bounded by the $P_{\rm GI} \simeq P_\sigma$ condition. This is in agreement with the results of Ferraz-Mello et al. (1998) who argued that even a near-resonant state of $P_{\rm GI}$ and P_σ can enhance the chaotic diffusion. However, it is clear that the number of asteroids surviving the smooth late migration depends mainly on the length of the time

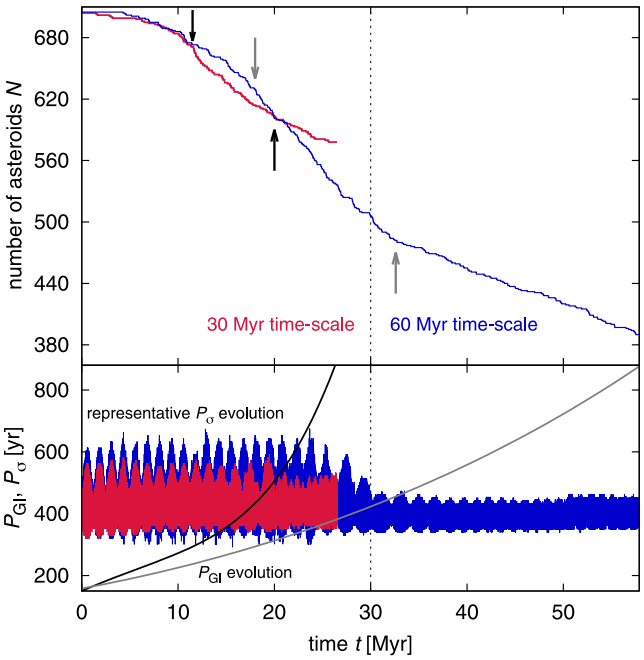

Figure 13. Results of two simulations of smooth late migration and its effects on the resonant population. Two runs with $t_{\rm fin} \simeq 27$ Myr (red and black curves and arrows) and $t_{\rm fin} \simeq 58$ Myr (blue and grey curves and arrows) are presented (migration time-scales $\tau_{\rm mig} = 30$ and 60 Myr were initially chosen but the integration is evaluated only until the GI period reaches 880 yr). Top: temporal evolution of the number N of test particles. Bottom: temporal evolution of the GI period $P_{\rm GI}$ and the libration period P_σ. The latter is plotted for two representative cases. The arrows in the top panel approximately mark the time period during which $P_{\rm GI} \simeq P_\sigma$. We note that 'real' $P_{\rm GI}$ evolves in an oscillatory manner but only with a small amplitude; a polynomial fit of the real $P_{\rm GI}$ evolution is plotted here for clarity.

interval during which $P_{\rm GI} \simeq P_\sigma$; the population is more depleted in the run with $t_{\rm fin} \simeq 58$ Myr.

With the aim to evaluate the result of the models with residual migration included, we first identified test particles which were located inside the stable islands at the time $t_{\rm fin}$. At this time, the orbital architecture of giant planets approximately corresponds to the observed one and therefore the identification of long-lived asteroids can be achieved using the *current* dynamical map. Finally, we derived expected numbers $N_{\rm A}^{\rm model}$ and $N_{\rm B}^{\rm model}$ of asteroids that should be observable in the stable islands after 4 Gyr of orbital evolution. For this purpose, we rescaled the initial population of test particles and we applied simple exponential dynamical decay law, exactly as in Section 3.2.

We calculated following values for asteroids larger than 5 km: $N_{\rm A}^{\rm model} = 0$–1 and $N_{\rm B}^{\rm model} = 40$–78 in the case of $t_{\rm fin} \simeq 27$ Myr and $N_{\rm A}^{\rm model} = 0$–1 and $N_{\rm B}^{\rm model} = 22$–42 in the case of $t_{\rm fin} \simeq 58$ Myr (while the observed values are $N_{\rm A}^{\rm obs} = 2$ and $N_{\rm B}^{\rm obs} = 71$). We can conclude that the hypothesis of resonant capture is still valid and explains the existence[6] of the long-lived population, if the giant planets finished their late stage migration on a time-scale comparable to $\tau_{\rm mig} \simeq 30$ Myr. Larger time-scales lead to a slower passage of the GI period over the values of the J2/1 libration period and this

[5] The results of simulations with primordial asteroids are not considered here, as these asteroids probably do not significantly contribute to the observed population.

[6] Although the values derived here do not overlap the observations in the case of island A, the difference is only one asteroid. We think that this discrepancy is not significant as we are comparing small numbers and the evolution is definitely stochastic.

in turn causes an enhanced depletion of the stable islands. Even in such a case, a significant part of the observed population should originate from the resonant capture.

5 COLLISIONAL MODELS

Our results of Section 3 and 4 imply that the long-lived J2/1 population was created by resonant capture during planetary migration. In this section, we further develop the framework of this hypothesis. We study collisional evolution of the J2/1 in order to confirm whether the SFD of the long-lived resonant asteroids can survive a time period of 4 Gyr in a non-stationary state. We thus have to also account for the epoch of the late heavy bombardment (LHB; Gomes et al. 2005; Levison et al. 2009) during which the trans-Neptunian disc was destabilized and the flux of cometary projectiles through the Solar system increased substantially.

In the following collisional models, three populations of minor Solar-system bodies are included: main-belt asteroids, trans-Neptunian comets and Zhongguos, i.e. we consider only a subset of the long-lived population. The reason for this simplification is that the observed SFDs of long-lived population and its dynamical subgroups share similar features (see Fig. 4), but Zhongguos have the steepest slope $\gamma = -5.1$. Solving an inverse problem, we aim to explain the formation of an initial SFD with an even steeper slope, which would evolve towards the observed one due to collisions over the 4 Gyr time span. Because of certain level of parametric freedom in collisional models, the same process of formation should also apply to Griquas with shallower observed SFD.

5.1 Intrinsic probabilities and impact velocities

As the first step in the construction of a collisional model, we compute the intrinsic probability P_i and the mean impact velocity V_i of colliding main-belt and long-lived resonant asteroids. We adopt the method of Bottke et al. (1994) based on a geometrical formalism of orbital encounters introduced by Greenberg (1982). To make our samples of orbits large enough, we input all long-lived orbits and the first 50 000 main-belt objects from the AstOrb catalogue.

We split the long-lived population into Zhongguos, Griquas with inclination $I \leq 8^\circ$ and Griquas with inclination $I > 8^\circ$ and calculate the intrinsic probability P_i and weighted mean impact velocity V_i for them, separately. Using this separation, we want to check if the intrinsic probabilities for Griquas may differ from Zhongguos significantly.

The results are summarized in the Table 3. For reference, Dahlgren (1998) computed $P_\mathrm{i} = 3.1 \times 10^{-18}\,\mathrm{km^{-2}yr^{-1}}$ and $V_\mathrm{i} = 5.28\,\mathrm{km\,s^{-1}}$ for collisions between main-belt asteroids. We can see that both Zhongguos and low-inclined Griquas have P_i and V_i only slightly higher than these reference values. This is caused by the moderate values of eccentricities in the J2/1 population.

Table 3. The intrinsic probability P_i and the mean impact velocity V_i for collisions of main-belt and long-lived J2/1 asteroids.

Colliding populations	P_i ($10^{-18}\,\mathrm{km^{-2}yr^{-1}}$)	V_i ($\mathrm{km\,s^{-1}}$)
Zhongguos versus MB	3.82	5.36
Griquas ($I \leq 8^\circ$) versus MB	3.65	5.52
Griquas ($I > 8^\circ$) versus MB	1.81	7.57
Average	3.09	6.15

The orbits then more likely intersect with those in the main belt. The higher collisional velocity is also plausible because we are comparing an outer main-belt population with the rest of the main belt.

On the other hand, Griquas with high inclinations can avoid intersecting some of main-belt orbits, thus their intrinsic probability is lower by about a factor of 2. Even at this point, we can conclude that the observed difference in slopes of SFDs (when Griquas and Zhongguos are separated) *cannot* be explained by the differences in P_i and V_i because the shallower SFD of Griquas would require higher P_i in order to collide more often.

5.2 Capture from the main-belt population

Let us ask a question whether the J2/1 SFD can originate from the main-belt SFD. We assume that the capture of the resonant population is *not* size dependent and thus the captured SFD resembles that of the main belt at the time of planetary migration, scaled down by a numerical factor. Our arbitrary choice of this factor is such that the number of the largest captured bodies is approximately the same as we observe in the J2/1 population. This allows us to immediately compare the slope of captured and observed SFD of Zhongguos.

The main belt itself was likely more populous 4 Gyr ago (by a factor of 3 according to Minton & Malhotra 2010) but has remained in a near-stationary collisional regime ever since (Bottke et al. 2005a). The only possible stage of evolution, which could have temporarily increased the slope of the main-belt SFD, was the LHB. We therefore investigate this early period of collisions between the main belt and trans-Neptunian comets. We focus on diameters $D < 25\,\mathrm{km}$ to see whether the steepness in this interval can be instantaneously increased – if so, a population captured from such SFD would adopt that slope.

We use the BOULDER code (Morbidelli et al. 2009) to construct a suitable collisional model. We setup initial SFDs by a piecewise power-law function which is characterized by three differential slope indices q_a, q_b and q_c in the intervals of diameters $D > D_1$, (D_2, D_1) and $D < D_2$, respectively. The SFD is normalized by setting the number N_norm of bodies larger than D_1. The following values are used in the case of the main-belt SFD: $D_1 = 100\,\mathrm{km}$, $D_2 = 14\,\mathrm{km}$, $q_\mathrm{a} = -5.0$, $q_\mathrm{b} = -2.3$, $q_\mathrm{c} = -3.5$, $N_\mathrm{norm} = 1110$. A few $D \sim 1000\,\mathrm{km}$ asteroids are added in order to properly reproduce the present state. Using the same assumptions as Brož et al. (2013), the cometary disc is characterized as: $D_1 = 100\,\mathrm{km}$, $q_\mathrm{a} = -5.0$, $q_\mathrm{b} = q_\mathrm{c} = -3.0$, $N_\mathrm{norm} = 5 \times 10^7$.

Because the evolution of the trans-Neptunian disc is dominated by its fast dynamical dispersion, the intrinsic probability $P_\mathrm{i}(t)$ and mean impact velocity $V_\mathrm{i}(t)$ of collisions with comets are time-dependent quantities. The temporal evolution of $P_\mathrm{i}(t)$ and $V_\mathrm{i}(t)$, which was derived in Brož et al. (2013), is shown in Fig. 14. Brož et al. (2013) also argued that it is necessary to modify this dependence in order to mimic the effects of spontaneous cometary break-ups due to various physical processes. Regarding these effects, they derived quantities $\tilde{P}_\mathrm{i}(t) = P_\mathrm{i}(t)/3$ and $\tilde{V}_\mathrm{i}(t) = V_\mathrm{i}(t)/1.5$ as a feasible modification.

The specific energy $Q^\star_\mathrm{D}$ required to disperse 50 per cent of the shattered target is described by the polynomial scaling law (Benz & Asphaug 1999)

$$Q^\star_\mathrm{D}(r) = \frac{1}{q_\mathrm{fact}} \left(Q_0 r^a + B\rho r^b \right) , \quad (8)$$

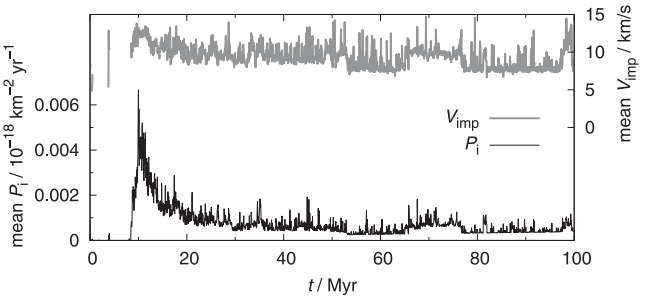

Figure 14. Temporal evolution of the intrinsic probability $P_i(t)$ (bottom curve) and the mean impact velocity $V_i(t)$ (top curve) for collisions between trans-Neptunian comets and main-belt asteroids, as it was calculated in Brož et al. (2013). We emphasize that we modify these dependences by numerical factors to allow for realistic lifetimes of comets. The values $P_i/3$ and $V_i/1.5$ serve as an input for our models.

Table 4. Material parameters ρ, Q_0, a, B, b and q_{fact} of the polynomial scaling law (see equation 8) adopted from Benz & Asphaug (1999). The first line is used in the case of main-belt or resonant asteroids and the second line is used for comets.

ρ (g cm^{-3})	Q_0 (erg g^{-1})	a	B (erg g^{-1})	b	q_{fact}
Basalt:					
3.0	7×10^7	−0.45	2.1	1.19	1.0
Water ice:					
1.0	1.6×10^7	−0.39	1.2	1.26	3.0

where r denotes the target's radius in cm. Material parameters ρ, Q_0, a, B, b and q_{fact} for basaltic rock (used for asteroids) and water ice (used for comets) are listed in Table 4.

We simulated the collisional evolution for a time period of 10 Myr in which $P_i(t)$ reaches its maximum (see Fig. 14 and top panel of Fig. 15). The flux of cometary projectiles induced by ongoing planetary migration reaches its climax and strongly affects the main-belt SFD. We performed 100 numerical realizations of the model with different seeds of the built-in random-number generator to account for stochasticity of the evolution and possible low-probability break-ups. At the end of the simulation, we assume the resonant capture takes place with the efficiency factor 10^{-4}. The steep part of the captured SFD can be characterized by the slope $\gamma = -3.0$. Although the region of the km-sized bodies is steeper with respect to the initial state of the main-belt SFD, it is not steep enough to reach the slope of the SFD of observed Zhongguos. We thus consider this scenario unlikely.

5.3 Catastrophic disruption of a captured parent body

From the result of the previous section, it is obvious that a different explanation of the steep initial SFD is needed. Here we test the possibility that a large parent body was captured inside the 2:1 resonance by chance, it was subsequently disrupted and its fragments formed a family.

We first use a stationary model to investigate the probability of such a catastrophic break-up event. As a prerequisite, we estimated a lower limit of the parent body size D_{PB}. To achieve that, we searched the outcomes of hydrodynamic disruption models in Durda et al. (2007) and Benavidez et al. (2012) for SFDs which have approximately the same slope as the observed SFD of Zhongguos. We rescaled the sizes of synthetic asteroids in these data sets so that

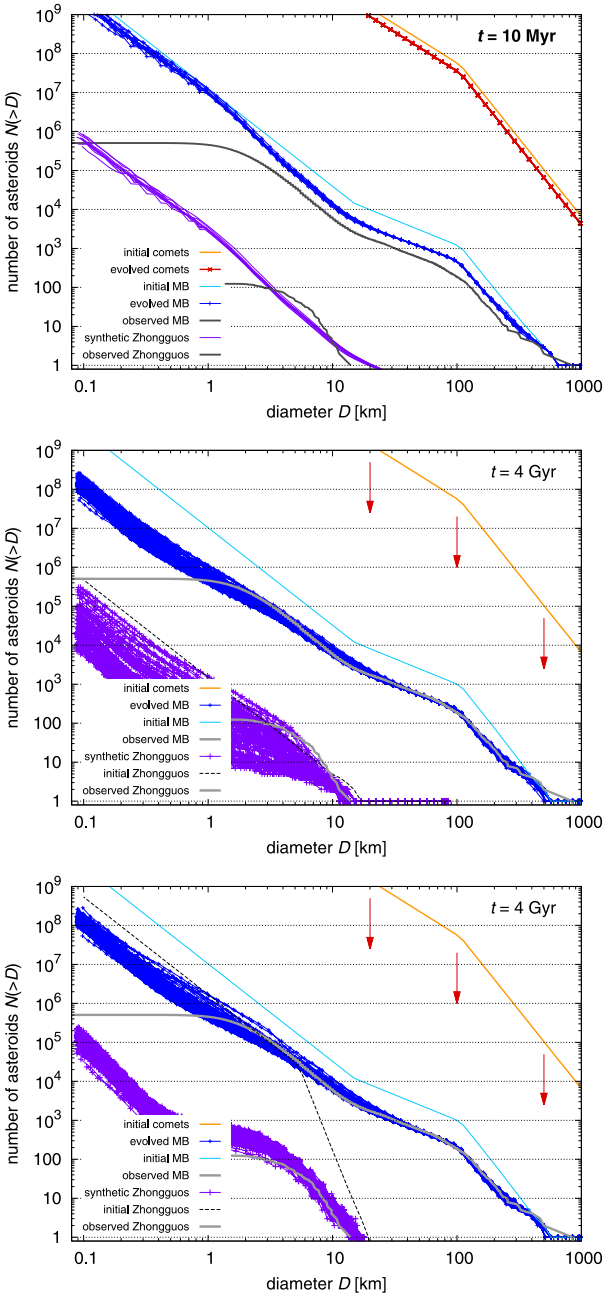

Figure 15. Results of collisional models created with the BOULDER code, plotted as temporal evolution of the SFDs. Description of individual curves is given in the legend of each plot. The evolving curves are displayed in the time of the simulation t, which is also shown. Top: synthetic Zhongguos are created by capture from the main-belt background population affected by collisions with trans-Neptunian comets (see also Section 5.2). Middle: the situation from top-left panel is reproduced, but a single $D \simeq 100$ km asteroid is added to Zhongguos and we study the possibility of its catastrophic break-up over 4 Gyr (see also Section 5.3). Bottom: we demonstrate what parameters of the initial SFD of Zhongguos are needed in order to evolve it towards the observed one due to collisions (see Section 5.4 for discussion).

the diameter of the largest remnant would correspond approximately to the size of (3789) Zhongguo. We selected all reasonable fits and derived range of admissible values $D_{PB} \in (50, 120)$ km with the median value $\tilde{D}_{PB} = 70$ km.

We then use the following relation expressing the number N_{col} of catastrophic disruptions of parent bodies with the diameter D_{PB} due

Table 5. The results of a stationary collisional model: the number $N_{\rm col}$ of catastrophic break-ups of a parent body with the diameter $D_{\rm PB}$ over 4 Gyr time span. We also list the minimal size $d_{\rm disrupt}$ and the number $N_{\rm project}$ of suitable projectiles.

$D_{\rm PB}$ (km)	$d_{\rm disrupt}$ (km)	$N_{\rm project}$	$N_{\rm col}$
50	6	25 821	0.18
70	9	7837	0.10
100	15	2589	0.07
120	19	1777	0.07

to collisions with a population of projectiles:

$$N_{\rm col} = P_{\rm i} N_{\rm PB} N_{\rm project} \frac{D_{\rm PB}^2}{4} \Delta t \,, \quad (9)$$

where $P_{\rm i}$ denotes the intrinsic probability, $N_{\rm PB}$ is the number of parent bodies, $N_{\rm project}$ is the number of projectiles capable of disrupting the parent body and Δt is the considered time span.

Since there are *no* large bodies observed in the current J2/1 population, we assume $N_{\rm PB} = 1$. To provide the lower limit on the diameter of the projectiles $d_{\rm disrupt}$, we use the model of Bottke et al. (2005b) in combination with the scaling law given by equation (8) (Benz & Asphaug 1999). We then take $N_{\rm project}$ for different values of $d_{\rm disrupt}$ as the number of main-belt asteroids with diameters $D \geq d_{\rm disrupt}$. Several resulting values of $N_{\rm col}$ over $\Delta t = 4$ Gyr time span are given in Table 5. It turns out that the probability of a catastrophic disruption is $\leq$18 per cent when considering a single target only.

Note that a more realistic case should take into consideration that there is no observable evidence of a collisional cluster, thus the hypothetical break-up event must have occurred more than 1 Gyr ago (Brož et al. 2005). Of course, one should also account for the influence of cometary flux during LHB which can temporarily increase the rate of collisions but also tends to speed up the evolution of SFDs.

We therefore test the possibility of a catastrophic break-up once again in the more sophisticated framework of the BOULDER code and we also check the influence of comets. The set-up for main-belt asteroids and comets is the same as in Section 5.2, as well as the SFD of synthetic Zhongguos, which is only modified by adding a single $D \simeq 100$ km asteroid. The intrinsic probability and the mean impact velocity for MB versus Zhongguos collisions are taken as the average of values from Table 3. We simulated 4 Gyr of collisional evolution.

The middle panel of Fig. 15 shows a set of 100 realizations of our model. At the beginning of the simulations, the synthetic population of Zhongguos is strongly affected by the cometary flux, which mostly causes cratering of the large body in the resonance. Moreover, a family-forming event takes place in a few runs. Simultaneously, the comets speed up the collisional evolution in and below the region of mid-sized asteroids. As a result, families inside the J2/1 are comminuted too fast and the steepness of their SFDs drops below the observed one.

When studying the family-forming events after the LHB, we focused only on cases with the size of the largest fragment (or remnant) $D_{\rm LF} \geq 10$ km to obtain a body similar to (3789) Zhongguo. In three such cases, which occurred at the time of simulation $t = 2.1$, 2.8 and 3.1 Gyr, a parent body with the diameter $D_{\rm PB} \simeq 85$ km was shattered into a family with the largest fragment having $D_{\rm LF} \simeq 18$ km and the largest remnant having $D_{\rm LR} \simeq 60$ km. Corresponding evolved SFDs match[7] the observed one, except for the presence of the parent-body remnant.

We can conclude that a family-forming event inside the 2:1 resonance is a very unlikely process because a complex set of constraints has to be satisfied: A major collision would have to occur despite its low probability, which is typically 10 per cent, as given by the stationary model, or 3 per cent, as derived from the more sophisticated model. The created SFD would have to be very steep, preferably without presence of a parent-body remnant. If the remnant was present, one would have to rely on its subsequent elimination due to dynamical depletion because there is no large asteroid observed in the J2/1. Finally, the break-up would have to take place after the LHB, but early enough to allow for dispersion of the collisional cluster.

5.4 Capture from a family

Previous collisional models imply that it is difficult to explain the steep SFD of Zhongguos by standard processes (such as direct capture from the background main-belt population or family-forming event) that could have occurred during resonant capture or later on. We thus employ a sort of 'reversed' method in this section. We first try to discover what parameters of the initial SFD are needed in order to obtain the observed one after 4 Gyr of collisional evolution. Then we discuss possible process which could have led to formation of such an SFD.

Using trial and error, we established the following initial SFD as an appropriate one: $D_1 = 10$ km, $D_2 = 5$ km, $q_{\rm a} = -6.6$, $q_{\rm b} = -6.6$, $q_{\rm c} = -3.5$, $N_{\rm norm} = 12$. The change of slope at D_2 is necessary to reasonably satisfy the mass conservation law. The main-belt and cometary SFDs are the same as in the previous models.

The result of 100 runs of the collisional code is displayed in bottom panel of Fig. 15. The evolved SFD of the resonant population corresponds to the observed one very well. The steep parts have the same slope, the only difference can be seen in the region of small bodies where the synthetic SFD is abundant. But one has to realize that the observed SFD is probably biased in this region.

The mechanism responsible for creation of the high initial slope may be the following (and it is related to the effect described in Carruba, Aljbaae & Souami 2014). Let us assume resonant capture from a hypothetical outer main-belt family instead of capture from the background main-belt population. The stable islands are able to capture only a fraction of this family because jump of the resonance is thought to be fast (it does not sweep through the resonance), the capture efficiency is limited (see Section 3.2), and also the width of the islands in semimajor axis is relatively small (see e.g. Fig. 1). If the captured part of the family is located farther away from the original position of the parent body, its SFD will be very steep because smaller fragments have higher ejection velocities and therefore land at orbits that are more distant from the parent body.

We employed a simple Monte Carlo test to investigate the described possibility. We generated a uniform distribution of 10 000 test particles satisfying the bounds $2.52 \leq a \leq 2.70$ au and $\log(|a - a_{\rm c}|/2 \times 10^{-4})/0.2 \leq H \leq 16$ in the (a, H) plane where

[7] In fact, the SFDs resulting from our simulations lie slightly below the observed case but this discrepancy can be easily removed assuming a bit larger parent body.

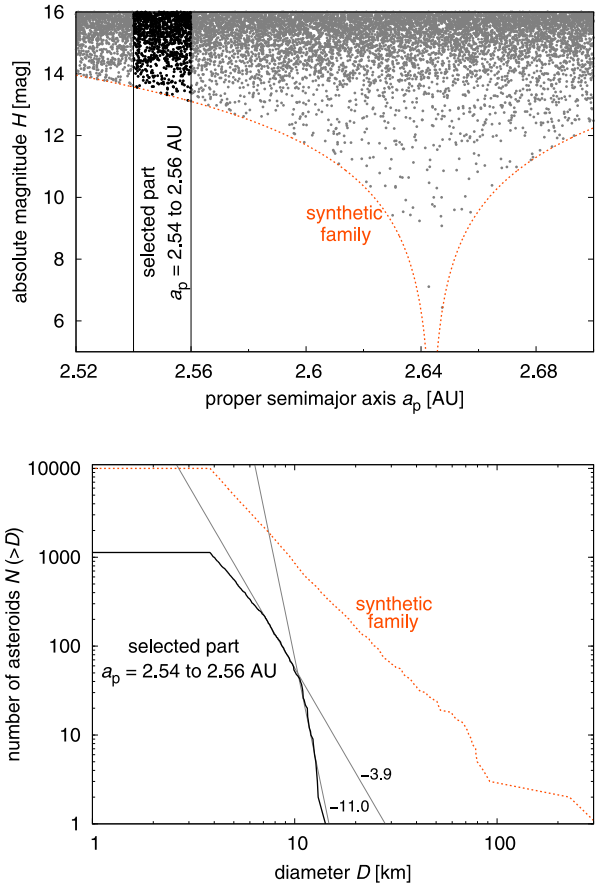

Figure 16. Dependence of the absolute magnitude H on the proper semimajor axis a_p for a synthetic family (top panel). The family is used in a simple Monte Carlo test, in which we study how the shape of the SFD changes if we select only a part of the family. An example, for the part of the family bordered by the vertical lines, is given in the bottom panel. We compare cumulative SFDs of the entire synthetic family (dashed curve) and of its part (solid curve). The steep segments are approximated with a power-law function and obtained slope indices are shown for reference.

$a_c \simeq 2.64$ au is value of the central semimajor axis and H is the absolute magnitude. Finally, we assigned diameters D to the test particles on the basis of the H distribution, assuming single value of the geometric albedo $p_V = 0.05$ throughout our sample. This way we created a synthetic family (similar e.g. to Eunomia family). Then we randomly moved a $\Delta a = 0.02$ au window in the semimajor axis over the collisional cluster and we monitored the SFDs in the successively selected regions.

An example is given in Fig. 16. Obviously, extremely high slope can be reached by this process. The resulting slope is well above the estimated lower limit which is needed for the initial SFD of Zhongguos. Note that this mechanism does not require the family *itself* to have steep SFD. The steepness is achieved afterwards by selective resonant capture from an appropriate region.

Finally, we remark that an interesting link can be found between the hypothesis of capture from a family and our dynamical simulations. In Section 3.2, we argued that a source population for resonant capture should contain greater number of asteroids with low inclination in order to explain the observed high concentration of low-I B-island bodies. Thus we can conclude that if the hypothetical outer main-belt family was indeed captured, it probably must have been located on low inclinations.

6 CONCLUSIONS

Let us briefly review the content of this paper. We updated the population of asteroids residing in the 2:1 mean-motion resonance with Jupiter using recent observational data. The new list of resonant objects now contains 370 bodies, which can be divided on the basis of their mean dynamical lifetime to 140 short-lived and 230 long-lived asteroids. Our revision of physical properties of the resonant population is generally in agreement with the conclusions of previous studies; new result is our estimate of the mean albedo $\bar{p}_V = (0.08 \pm 0.03)$, based on the data from the WISE data base.

The long-term dynamics of the two quasi-stable islands A and B was studied, using the results of Skoulidou et al. (in preparation) who took into account also the perturbations induced by the terrestrial planets and the semimajor axis drift caused by the Yarkovsky effect. The population in the islands decays exponentially, but the escape rate is significantly faster in island A, the e-folding times being 0.57 Gyr for island A and 0.94 Gyr for island B. Hence, the dynamical evolution on Gyr-long time-scales results into differential depletion of the islands, which is certainly one of the reasons for the observed asymmetric A/B population ratio.

The primary goal of this paper was to explain the formation of the long-lived population, satisfying the observational constraints. We tested two hypotheses:

(i) capture from the outer main belt,
(ii) survival of primordial long-lived resonant asteroids,

both in the framework of the five giant planets migration scenario (Nesvorný & Morbidelli 2012) with a jumping-Jupiter instability.

Our simulations of the instability imply that both processes could have been at work. The capture itself, together with subsequent differential depletion due to long-term dynamical evolution, can explain the observed population in both islands, if we assume that the number of asteroids in the main belt 4 Gyr ago was *three times larger* than the current one, as suggested by Minton & Malhotra (2010). Namely, the numbers of asteroids with $D \geq 5$ km, which should survive to this day, are $N_A^{model} = 1$–3 and $N_B^{model} = 62$–121, as predicted by our model. For comparison, the observed numbers are $N_A^{obs} = 2$ and $N_B^{obs} = 71$.

We also modelled the late residual planetary migration to check on the effect of possible resonance between the libration period in the 2:1 commensurability and the raising period of Jupiter–Saturn GI. The impact of this effect on the long-lived population depends on the time-scale of the late migration. If the time-scale was $\simeq 30$ Myr (which corresponds with the scenarios in Nesvorný & Morbidelli 2012), the destabilization of the islands would be weak enough for the captured population to survive in a state similar to the observations. More specifically, if we account for the effect of GI in our model, the resulting values are $N_A^{model} = 0$–1 and $N_B^{model} = 40$–78. If the time-scale was $\simeq 60$ Myr, the chaos in the stable islands would be intensified for longer period of time and the depletion of the captured population would be more significant, leading to $N_A^{model} = 0$–1 and $N_B^{model} = 22$–42.

In the case of primordial resonant objects, we discovered that approximately 1 per cent of A-island and 4 per cent of B-island asteroids survive Jupiter's jump on long-lived orbits. However, we argued that the primordial asteroids probably do not contribute to the observed population at all. The reason is that the primordial population would have to exhibit particle density larger than the one proposed by Minton & Malhotra (2010) by a factor of 10, in order to survive 4 Gyr of post-migration dynamical evolution. Such particle

density would create a gradient with respect to the neighbouring main belt which we assume dubious.

Finally, by creating several collisional models, we demonstrated that the observed steep SFD of the long-lived asteroids cannot be explained by capture from the background main-belt SFD, affected by the LHB. We also proved that a family-forming catastrophic disruption inside the J2/1 is very unlikely.

Our main conclusion is that the long-lived J2/1 population was probably formed by capture from a hypothetical outer main-belt family during Jupiter's jump. If this is the case, then the long-lived asteroids in the 2:1 resonance with Jupiter represent the oldest identifiable remnants of a main-belt asteroidal family.

There are several improvements that are needed to conclude the debate on the long-lived population in the 2:1 resonance and its origin. For example, it is appropriate to assess the possibility of the Themis family formation event as a contributor to the resonant population. Although we did not study this hypothesis in detail, we summarized several results of our preliminary tests in Appendix A. Our simulations suggest that this possibility is not viable and this in turn supports the hypothesis of resonant capture.

Other improvements of our work might include a development of a self-consistent model of both dynamical and collisional evolution of long-lived asteroids. Finally, we suggest to study the hypothetical primordial population in the epoch *before* the jumping-Jupiter instability in order to properly estimate primordial particle density inside the stable islands.

ACKNOWLEDGEMENTS

The work of OC and MB has been supported by the Grant Agency of the Czech Republic (grant no. 13-01308S) and by Charles University in Prague (project GA UK no. 1062214; project SVV-260089). The work of DN was supported by NASA's Solar System Workings programme. We thank an anonymous reviewer for valuable comments, which improved the final version of the paper.

REFERENCES

Benavidez P. G., Durda D. D., Enke B. L., Bottke W. F., Nesvorný D., Richardson D. C., Asphaug E., Merline W. J., 2012, Icarus, 219, 57
Benz W., Asphaug E., 1999, Icarus, 142, 5
Bottke W. F., Nolan M. C., Greenberg R., Kolvoord R. A., 1994, Icarus, 107, 255
Bottke W. F., Durda D. D., Nesvorný D., Jedicke R., Morbidelli A., Vokrouhlický D., Levison H., 2005a, Icarus, 175, 111
Bottke W. F., Durda D. D., Nesvorný D., Jedicke R., Morbidelli A., Vokrouhlický D., Levison H. F., 2005b, Icarus, 179, 63
Bowell E., 2012, The Asteroid Orbital Elements Database. Available at: ftp://ftp.lowell.edu/pub/elgb/astorb.html
Brož M., Morbidelli A., 2013, Icarus, 223, 844
Brož M., Vokrouhlický D., 2008, MNRAS, 390, 715
Brož M., Vokrouhlický D., Roig F., Nesvorný D., Bottke W. F., Morbidelli A., 2005, MNRAS, 359, 1437
Brož M., Vokrouhlický D., Morbidelli A., Nesvorný D., Bottke W. F., 2011, MNRAS, 414, 2716
Brož M., Morbidelli A., Bottke W. F., Rozehnal J., Vokrouhlický D., Nesvorný D., 2013, A&A, 551, A117
Carruba V., Aljbaae S., Souami D., 2014, ApJ, 792, 46
Dahlgren M., 1998, A&A, 336, 1056
DeMeo F. E., Carry B., 2013, Icarus, 226, 723
Dohnanyi J. S., 1969, J. Geophys. Res., 74, 2531
Durda D. D., Bottke W. F., Nesvorný D., Enke B. L., Merline W. J., Asphaug E., Richardson D. C., 2007, Icarus, 186, 498
Farinella P., Gonczi R., Froeschle C., 1993, Icarus, 101, 174
Ferraz-Mello S., Michtchenko T. A., Roig F., 1998, AJ, 116, 1491
Franklin F. A., 1994, AJ, 107, 1890
Gomes R., Levison H. F., Tsiganis K., Morbidelli A., 2005, Nature, 435, 466
Greenberg R., 1982, AJ, 87, 184
Harris A. W., 1998, Icarus, 131, 291
Henrard J., Watanabe N., Moons M., 1995, Icarus, 115, 336
Kirkwood D., 1867, Meteoric Astronomy: A Treatise on Shooting-stars, Fireballs, and Aerolites. J. B. Lippincott & co., Philadelphia
Knežević Z., Milani A., 2003, A&A, 403, 1165
Laskar J., 1994, A&A, 287, L9
Laskar J., Robutel P., 2001, Celest. Mech. Dyn. Astron., 80, 39
Levison H. F., Duncan M. J., 1994, Icarus, 108, 18
Levison H. F., Bottke W. F., Gounelle M., Morbidelli A., Nesvorný D., Tsiganis K., 2009, Nature, 460, 364
Masiero J. R. et al., 2011, ApJ, 741, 68
Masset F., Snellgrove M., 2001, MNRAS, 320, L55
Michtchenko T., Ferraz-Mello S., 1997, Planet. Space Sci., 45, 1587
Minton D. A., Malhotra R., 2010, Icarus, 207, 744
Moons M., Morbidelli A., Migliorini F., 1998, Icarus, 135, 458
Morbidelli A., 1997, Icarus, 127, 1
Morbidelli A., Crida A., 2007, Icarus, 191, 158
Morbidelli A., Moons M., 1993, Icarus, 102, 316
Morbidelli A., Bottke W. F., Nesvorný D., Levison H. F., 2009, Icarus, 204, 558
Morbidelli A., Brasser R., Gomes R., Levison H. F., Tsiganis K., 2010, AJ, 140, 1391
Murray C. D., 1986, Icarus, 65, 70
Nesvorný D., Ferraz-Mello S., 1997, A&A, 320, 672
Nesvorný D., Morbidelli A., 2012, AJ, 144, 117
Nesvorný D., Vokrouhlický D., Morbidelli A., 2013, ApJ, 768, 45
O'Brien D. P., Morbidelli A., Bottke W. F., 2007, Icarus, 191, 434
Parker A., Ivezić Ž., Jurić M., Lupton R., Sekora M. D., Kowalski A., 2008, Icarus, 198, 138
Press W. R., Teukolsky S. A., Vetterling W., Flannery B. P., 2007, Numerical Recipes: The Art of Scientific Computing. Cambridge Univ. Press, Cambridge
Rabe E., 1959, AJ, 64, 53
Roig F., Ferraz-Mello S., 1999, Planet. Space Sci., 47, 653
Roig F., Nesvorný D., Ferraz-Mello S., 2002, MNRAS, 335, 417
Schubart J., 1964, SAO Special Report 149, Long-Period Effects in Nearly Commensurable Cases of the Restricted Three-Body Problem, Smithsonian Astrophys. Obser., Cambridge, MA
Schweizer F., 1969, AJ, 74, 779
Skoulidou D. K., Tsiganis K., Varvoglis H., 2014, in Knežević Z., Lemaître A., eds, Proc. IAU Symp. 310, Complex Planetary Systems. Cambridge Univ. Press, Cambridge, p. 178
Standish E. M., 2004, A&A, 417, 1165
Tsiganis K., Knežević Z., Varvoglis H., 2007, Icarus, 186, 484
Wisdom J., 1987, Icarus, 72, 241
Zappalà V., Bendjoya P., Cellino A., Farinella P., Froeschlé C., 1995, Icarus, 116, 291

APPENDIX A: CONTRIBUTION OF THE THEMIS FAMILY EJECTA TO THE LONG-LIVED POPULATION

We shall briefly discuss a possible role of neighbouring Themis family in creation of the long-lived resonant population. Although Brož et al. (2005) demonstrated that the fragments from Themis family cannot be transported to the stable islands by the Yarkovsky semi-major axis drift, a possibility of direct injection during the Themis family formation event is still an open question. During the formation, fragments ejected at high velocities ($v_{\rm ej} \simeq 400\,{\rm m\,s^{-1}}$, or more) may fall directly in the J2/1 resonance and thus contribute somehow to the stable population. There are several caveats, however.

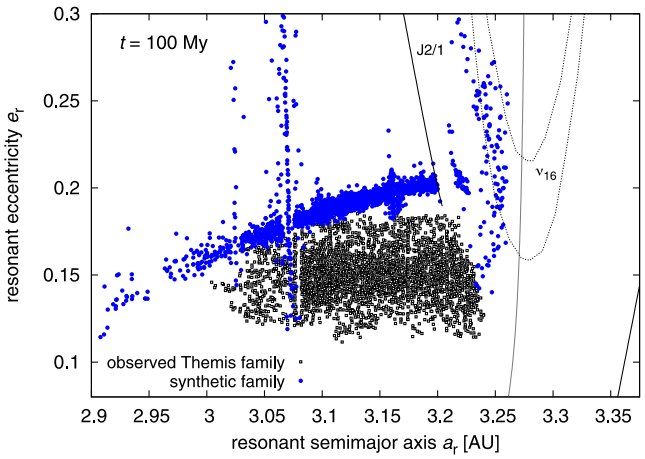

Figure A1. A simulation of a synthetic Themis-like family formation event. The figure represents the state 100 Myr after the break-up. The orbital distribution of observed Themis family is displayed in the proper elements (black squares), while the orbital distribution of the synthetic family is displayed in the resonant elements (blue circles). This causes the mutual shift in eccentricity. Note the differences in extent of both families and the eccentricity dispersion beyond the 11:5 mean-motion resonance with Jupiter.

(i) One has to assume that a substantial part of fragments ($\simeq$10 per cent) have very large ejection velocities with respect to (24) Themis, or the respective parent body with $D_{\rm PB} \simeq 400$ km. We tried to use an 'extreme' size-independent velocity field prescribed by Farinella, Gonczi & Froeschle (1993) relation, with parameters $v_{\rm esc} = 170\,{\rm m\,s^{-1}}$ and $\alpha = 3.25$. Then up to $N(D > 5\,{\rm km}) = 10$–30 fragments land within island B, according to our tests. This number should be further decreased by a subsequent long-term orbital evolution, as Themis family is (2.5 $\pm$ 1.0) Gyr old (Brož et al. 2013). Let us also note that the collisional evolution of resonant bodies was accounted for automatically, as we did this simulation with the currently observed SFD of Themis family.

(ii) At the same time, it is required that the break-up takes place when the true anomaly $f_{\rm imp} \simeq 0^\circ$ for this ejection scenario to work; otherwise, the number of objects landing in the islands decreases as well. But this particular impact geometry does *not* seem to be compatible with the observed shape of Themis family, namely with a large eccentricity dispersion of the family below the J11/5 resonance, at $a_{\rm p} = 3.03$ au (see Fig. A1).

(iii) Starting with a more reasonable size-dependent velocity field – as used in Brož & Morbidelli (2013) for Eos family, which has a similar parent body size – makes the contribution to the long-lived population as low as $N(D > 5\,{\rm km}) = 2$.

(iv) There is no way to explain the existence of asteroids in island A by the ejection, both the eccentricities and inclinations of the observed A-island objects are too large. Therefore, the ejection from Themis is not a viable hypothesis in the case of island A.

This paper has been typeset from a TEX/LATEX file prepared by the author.